Development of *N*-(1-Adamantyl)benzamides as novel Anti-inflammatory Multitarget Agents acting as Dual Modulators of Cannabinoid CB2 Receptor and Fatty Acid Amide Hydrolase

Francesca Intranuovo,[1] Leonardo Brunetti,[1] Pietro DelRe,[2] Giuseppe Felice Mangiatordi,[2] Angela Stefanachi,[1] Antonio Laghezza,[1] Mauro Niso,[1] Francesco Leonetti,[1] Fulvio Loiodice,[1] Alessia Ligresti,[3] Magdalena Kostrzewa,[3] Jose Brea,[4,5] Maria Isabel Loza,[4,5] Eddy Sotelo,[6] Michele Saviano,[7] Nicola Antonio Colabufo,[1] Chiara Riganti,[8] Carmen Abate[1,2]* and Marialessandra Contino[1]*

Affiliations

[1] *Dipartimento di Farmacia-Scienze del Farmaco, Università degli Studi di Bari ALDO MORO, via Orabona 4, 70125, Bari, Italy;*

[2] *Institute of Crystallography, National Research Council of Italy, Via Amendola, 122/o, 70126 Bari, Italy;*

[3] *Institute of Biomolecular Chemistry, National Research Council of Italy, Via Campi Flegrei 34, 80078 Pozzuoli (Na), Italy;*

[4] *Innopharma Screening Platform, BioFarma Research Group, Center for Research in Molecular Medicine and Chronic Diseases (CIMUS), University of Santiago de Compostela, 15782, Santiago de Compostela, Spain;*

[5] *Department of Pharmacology, Pharmacy and Pharmaceutical Technology. School of Pharmacy. University of Santiago de Compostela, 15782, Santiago de Compostela, Spain*

[6] *ComBioMed Research Group, Centro de Química Biológica y Materiales Moleculares (CIQUS) University of Santiago de Compostela, 15782, Santiago de Compostela, Spain;*

[7] *Institute of Crystallography, National Research Council of Italy, Via Vivaldi, 43, 81100 Caserta, Italy;*

[8] *Dipartimento di Oncologia, Università degli Studi di Torino, 10126, Torino, Italy*

Abstract

Cannabinoid type 2 receptor (CB2R), belonging to the endocannabinoid system, is overexpressed in pathologies characterized by inflammation and its activation counteracts inflammatory states. Fatty Acid Amide Hydrolase (FAAH) is an enzyme responsible for the degradation of the main endocannabinoid anandamide; thus, the simultaneous CB2R activation and FAAH inhibition may be a synergistic anti-inflammatory strategy. Encouraged by Principal Component Analysis (PCA) data identifying a wide chemical space shared by CB2R and FAAH ligands, we designed a small library of adamantyl-benzamides, as potential dual agents, CB2R agonists and FAAH inhibitors. The new compounds were tested for their CB2R affinity/selectivity and CB2R and FAAH activity. Derivatives

13, **26** and **27**, displaying the best pharmacodynamic profile as CB2R full agonists and FAAH inhibitors, decreased pro-inflammatory and increased anti-inflammatory cytokines production. Molecular docking simulations complemented the experimental findings by providing a molecular rationale behind the observed activities. These multitarget ligands constitute promising anti-inflammatory agents.

INTRODUCTION

Cannabinoid receptor subtype 2 (CB2R) belongs to the endocannabinoid system (ECS) recently defined as part of a wide and more complex system claimed as Endocannabinoidome.[1] This is an expanded ECS[2] made of several receptors that include the canonical cannabinoid receptor subtype CB1 (CB1R) and CB2 (CB2R) and other non-canonical ones,[3] twenty enzymes involved in the biosynthesis and degradation of endocannabinoids and more than one hundred lipid mediators.[4] CB2R has increasingly gained attention in the last years since its activation can mitigate neuroinflammatory events without eliciting psychotropic actions, that are a limiting factor for drugs targeting CB1R.[5] CB2R is an emerging target as it is involved in several pathologies characterized by an inflammatory state such as cancer, neurodegeneration and also COVID-19.[6–14] Recently, a deep learning algorithm for automated design of druglike analogues, named DeLA-Drug, was successfully developed and applied to CB2R.[15] Differently from CB1R, mainly present at the Central Nervous System (CNS) level, CB2R is physiologically located in the immune system and is overexpressed in pathological inflammatory states. It is widely reported that CB2R activation leads to microglia polarization from the M1-state (pro-inflammatory microglia phenotype) to the M2-state (anti-inflammatory microglia phenotype). The M1 to M2 polarization induced by CB2R activation in response to stimuli results in an anti-inflammatory action as final effect. In 2007, Ashton and Glass found CB2R up-regulation in the activated microglia due to brain injury and high CB2R levels in the microglia of human Alzheimer's disease (AD) brain.[16] In 2003, Benito and colleagues found high expression of CB2R and Fatty Acid Amide Hydrolase (FAAH), the enzyme responsible for the degradation of the main endocannabinoid anandamide and related signaling lipids, in neuritic plaque-associated glia in the brains of AD patients, suggesting a potential involvement of these two targets in neurodegeneration.[17] Thus, pharmacological action on these two targets could be particularly advantageous to contrast inflammatory processes, since raised concentrations of anandamide also induce a reduction in the levels of pro-inflammatory cytokines, reactive oxygen species (ROS) and prostaglandins as a result of the activation of non-canonical endocannabinoid receptors like the vanilloid receptor TRPV1 and Peroxisome Proliferator-Activated Receptors (PPARs).[18] Notably, it has been demonstrated that the therapeutic effects of FAAH inhibitors often come free of the psychotropic side effects typical of phytocannabinoids, and FAAH inhibitors have proven to be generally safe, provided that they are non-covalent and that they are not indiscriminate inhibitors of brain serine hydrolases.[19,20] The activation of CB2R is likewise unrelated to psychotropic effects. This multitarget approach was recently adopted by Gado and co-workers who developed a new class of cannabinoid ligands, bearing a 6-aryl-1,2-dihydro-2-oxo-pyridine-3-carboxamide scaffold, that were tested for their ability to bind CBRs and to block anandamide uptake or FAAH activity. Nevertheless, a good compromise in terms of multiple activities towards these targets was not achieved.[21] Moreover, studies on natural products as *zingiber officinale* and *acmella oleracea*, acting on both CB2R and FAAH, proposed natural extracts acting on these two targets as natural anti-inflammatory strategy to be adopted mainly in pain management.[22] With the aim of challenging the existence of a common chemical space covered by CB2R and FAAH ligands, we followed an approach successfully proposed for designing dual CB2R/HDAC and CB2R/sigma-1 receptor compounds.[14] Importantly, the freely accessible repository ChEMBL[23] (version 30) contains curated experimental data concerning 1,020 and 406 compounds

displaying high affinity (IC_{50} or K_i values $\leq 1\mu M$) towards the human forms of CB2R and FAAH, respectively. As depicted in Figure 1, the projection of these compounds into the top two principal components (PCs) obtained from the computed physicochemical descriptors supports the hypothesis whereby a wide chemical space is shared by CB2R and FAAH ligands.
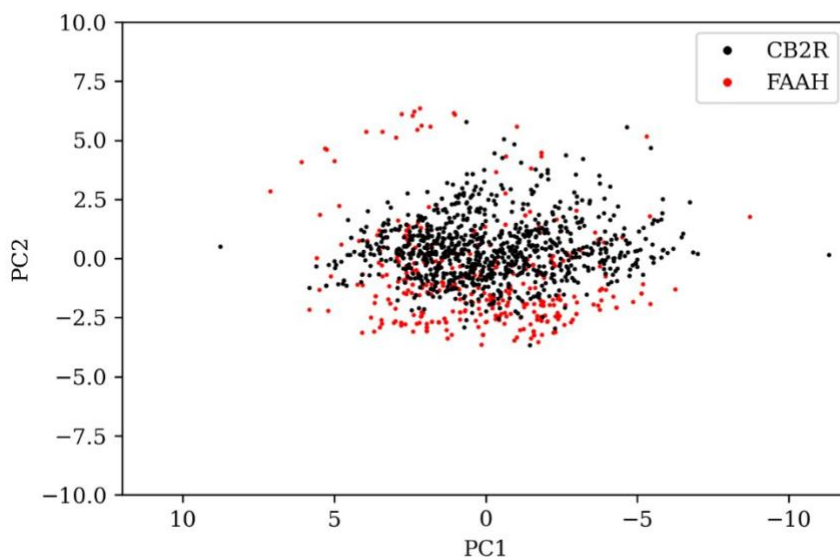
Figure 1. Projection of CB2R (black points) and FAAH (red points) high affinity (IC_{50} or $K_i \leq 1$ μM) compounds into the top two PCs obtained from 16 physicochemical descriptors. Note that PC1 and PC2 are plotted accounting for 70% of the total variance.

Encouraged by previous studies and by these preliminary PCA data, we designed a small library of new derivatives (**9**-**19**, **22**-**29**) as potential dual agents able to activate CB2R and inhibit FAAH according to a multitarget approach, in order to synergistically contrast the inflammatory cascade proper of pathologies such as cancer, neurodegeneration and COVID-19. For this purpose, we were inspired by the convenient-to-modify pyridine-3-carboxyamide CB2R pharmacophore explored by Lucchesi and co-workers (general formula in Figure 2, A).[24] We isosterically replaced the pyridine-3-carboxyamide core with a salicylamide one and the adamantane tricycle was inserted in place of the cycloalkanes, according to previous and robust SAfiR studies that relate the adamantylamine fragment to high CB2R affinity.[5] The absence, as well as the position of the phenolic group on the benzene ring, together with the corresponding alkoxy substituents (*i.e.* methoxy, benzyloxy, pentyloxy, cyclohexylmethoxy) were explored. The insertion of a bromine substituent and the pluri-substitution on the benzene ring were also investigated, in order to confirm hints from SAfiR and produce a dual CB2R agonist-FAAH inhibitor lead compound.
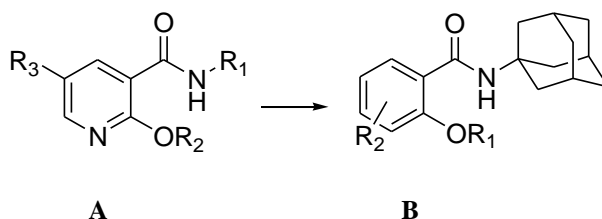
Figure 2. General formula of the derivatives published by Lucchesi et al[24] (**A**) and general formula of the planned dual compounds acting as CB2R agonists and FAAHIs (**B**).

The newly synthesized compounds **9-19** and **22-29** (general formula in Figure 2B) were assayed for their CB2R affinity and selectivity as well as for FAAH inhibition. For the most promising dual compounds, the CB2R activity profile (agonism or antagonism) and the ability to recruit β2-arrestin (functional selectivity) were further investigated, as well as their CB1R activity profile and mainly their impact on pro- and anti-inflammatory cytokines production, which was evaluated on monocytes and macrophages in basal and activated conditions.
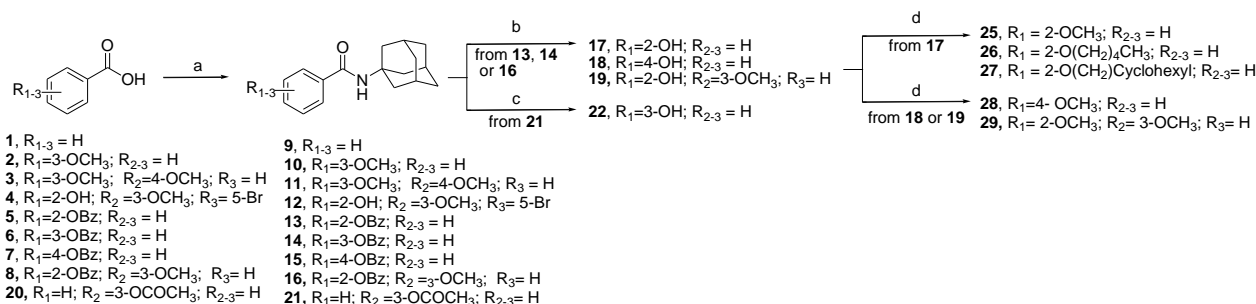
Considering the reported activity of salicylamides, as well as benzamides, as iron species chelating agents and the potential use of these ligands in a neuroprotective approach, all the derivatives were also tested for their ability to chelate iron ion species, to further clarify their therapeutic potential.[25,26] These findings allow us to suggest these ligands as first-in-class for the development of multitarget agents able to alleviate or prevent the inflammatory cascade that is the leading detrimental step in several severe diseases as neurodegeneration, cancer and COVID-19. The ability of the best compounds to permeate the Blood Brain Barrier (BBB) was also predicted and experimentally tested (see supporting information, 'P-glycoprotein interaction' section and Figure S1), demonstrating their capability to access the CNS.

RESULTS AND DISCUSSION

Chemistry

The synthetic pathway for all final compounds **9-19**, **22-29** is depicted in Scheme 1. The commercially available benzoic acids **1-4** and the synthesized acids **5-8**, upon activation with *N,N,N',N'*-tetramethyl-*O*-(1*H*-benzotriazol-1-yl)uronium hexafluorophosphate (HBTU), were reacted with 1-adamantylamine in the presence of *N,N*-Diisopropylethylamine (DIPEA) to provide the already known final benzamides **9**[27] and **10**,[28] and novel final amides **11-16**,[29] respectively. While the former amides were synthesized according to different procedures compared to the reported ones, the latter amides were obtained through the procedure described by Pasquini et al.[29] The synthesized benzoic acids used in this synthesis (i.e. **5-8**) were obtained with minor modifications to the previously published procedures,[30–32] from the commercially available 2-hydroxy, 3-hydroxy, 4-hydroxy and 2-hydroxy-3-methoxy benzoic acids, upon the simultaneous protection of the phenolic and carboxylic acid functions by benzylation with benzylbromide. The obtained derivatives underwent basic hydrolysis to provide the corresponding acids **5-8**. Subsequent hydrogenolysis of the *N*-adamantan-1-yl-(benzyloxy)benzamide **13-16** in the presence of Pd on carbon 10%, led to key compounds **17**, the already known **18**,[33] which was obtained through a different synthetic procedure, and **19**. The same hydrogenolytic conditions were unsuccessfully applied to the 3-benzyloxy derivative **14**. Thus, the phenolic function in the 3-hydroxybenzoic acid was protected by acetylation with acetic anhydride to provide the ester **20** that upon reaction with 1-adamatylamine, as for the other acids, provided the corresponding benzamide intermediate **21**. Hydrolysis of the ester function of this latter in the presence of $NaHCO_3$ provided the desired final amide **22**. The phenolic function of final benzamides **12**, and **17-19**, was alkylated with the appropriate alkyl halides to obtain final compounds **23-29**. The already known compounds **25** and **28** were obtained in a slightly different manner compared to the previously reported procedures.[28]

Scheme 1. Synthetic pathway for final benzamide derivatives **9-19** and **22-29**.
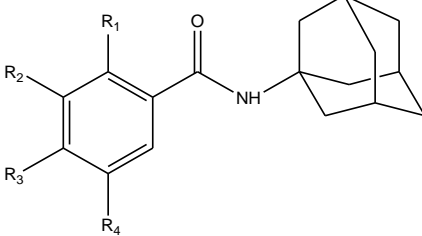

1, R$_{1-3}$ = H
2, R$_1$=3-OCH$_3$; R$_{2-3}$ = H
3, R$_1$=3-OCH$_3$; R$_2$=4-OCH$_3$; R$_3$ = H
4, R$_1$=2-OH; R$_2$ =3-OCH$_3$; R$_3$= 5-Br
5, R$_1$=2-OBz; R$_{2-3}$ = H
6, R$_1$=3-OBz; R$_{2-3}$ = H
7, R$_1$=4-OBz; R$_{2-3}$ = H
8, R$_1$=2-OBz; R$_2$ =3-OCH$_3$; R$_3$= H
20, R$_1$=H; R$_2$ =3-OCOCH$_3$; R$_{2-3}$= H

9, R$_{1-3}$ = H
10, R$_1$=3-OCH$_3$; R$_{2-3}$ = H
11, R$_1$=3-OCH$_3$; R$_2$=4-OCH$_3$; R$_3$ = H
12, R$_1$=2-OH; R$_2$ =3-OCH$_3$; R$_3$= 5-Br
13, R$_1$=2-OBz; R$_{2-3}$ = H
14, R$_1$=3-OBz; R$_{2-3}$ = H
15, R$_1$=4-OBz; R$_{2-3}$ = H
16, R$_1$=2-OBz; R$_2$ =$_3$-OCH$_3$; R$_3$= H
21, R$_1$=H; R$_2$ =3-OCOCH$_3$; R$_{2-3}$= H

17, R$_1$=2-OH; R$_{2-3}$ = H
18, R$_1$=4-OH; R$_{2-3}$ = H
19, R$_1$=2-OH; R$_2$=3-OCH$_3$; R$_3$= H

22, R$_1$=3-OH; R$_{2-3}$ = H

25, R$_1$ = 2-OCH$_3$; R$_{2-3}$ = H
26, R$_1$ = 2-O(CH$_2$)$_4$CH$_3$; R$_{2-3}$ = H
27, R$_1$ = 2-O(CH$_2$)Cyclohexyl; R$_{2-3}$= H

28, R$_1$=4- OCH$_3$; R$_{2-3}$ = H
29, R$_1$= 2-OCH$_3$; R$_2$= 3-OCH$_3$; R$_3$= H

Reagents and conditions: a) 1-Adamantanamine, HBTU, DIPEA, DMF anhydrous, 20 h, room temperature; b) H$_2$ 2.5 bar, Pd/Carbon 10%, MeOH, 48 h, room temperature; c) NaHCO$_3$, MeOH/H$_2$O, 2 h, room temperature; d) alkyl halide, K$_2$CO$_3$, acetone, 4 h, reflux.

Biology

CB2R affinity and selectivity. Results from radioligand binding assays are expressed as inhibition constants K_i values for CB2R and as K_i or displacement percentage at 1 μM for CB1R in Table 1.

The unsubstituted benzamide **9** is devoid of affinity at both the CBR subtypes and the insertion of the hydroxyl function either in position 2- or 3- on the benzene ring (**17** and **22**, respectively) also results in a total lack of CB2R and CB1R affinity. Only the 4-substituted analogue (**18**) recovers a certain CB2R affinity (K_i = 1060 nM), whereas the affinity at the CB1R is comparable to its isomers. Methylation of the hydroxyl function leads to the recovery of the CB2R affinity both in position 2 or 3 of the benzene ring (**25** and **10**, respectively) with K_i values in the three-digit nanomolar range (K_i = 387 nM for **25** and K_i = 510 nM for **10**). By contrast, the 4-substituted isomer **28** shows around 2-fold reduction of the affinity compared to its hydroxy counterpart **18**. No substantial change in the CB1R affinity is conferred by this substitution, with the three methoxy derivatives (**10**, **25** and **28**) displaying the same percentage of inhibition of their hydroxyl counterparts (**22**, **17** and **18**). Because of the improvement provided by the methylation of the hydroxyl function in position 2 or 3, we investigated with **19** whether the salicylamide derivative **17** could benefit of the 3-methoxy presence, also taking into consideration the superior metal chelating properties of the salicyl-amide. The CB2R nanomolar affinity displayed by **19** (K_i = 153.1 nM) confirmed the beneficial effect of the 3-methoxy substituent that is able to confer CB2R affinity also to compound **17** (absence of affinity). Accordingly, the 2,3-di-methoxy substitution leads to higher CB2R affinity values (**29**, K_i = 87.6 nM) in the absence of CB1R affinity. The same di-functionalization in 3- and 4- positions (**11**) does not lead to an improved affinity compared to the 4-methoxy counterpart (**28**), thus supporting the negative impact of the 4-methoxy substitution on the CB2R interaction. The increase in the CB2R affinity exerted by the methoxy group, in particular in 2-position, encouraged to explore other alkyl groups. In agreement with Lucchesi *et al.*,[24] benzylation of the hydroxyl function in 2-position leads to a striking recovery of the CB2R affinity (**13**, K_i = 14.8 nM) compared to the phenol counterpart (**17**), and a 26-fold increase compared to the methoxy counterpart (**25**). A partial recovery of the CB2R affinity is recorded also with the 3-benzyloxy derivative **14** (K_i = 313 nM), but no substantial improvement compared to the methoxy counterpart (**10**) is brought. On the other hand, the 4-

benzyloxy derivative **15** shows a 4-fold decrease in the CB2R affinity compared to its hydroxy-counterpart **18**, confirming the poor tolerance of alkoxy-substituents in that position. Thus, the 2-hydroxyl group has been alkylated with a *n*-pentyl chain (**26**) and a cyclohexylmethyl group (**27**), both resulting in nanomolar affinity (K_i = 10.8 nM and 20.1 nM, respectively), in line with the corresponding benzyloxy analogue **13**. All these 2-alkoxy groups, bigger than methoxy (**25**), confer a certain degree of CB1R affinity, mainly in a three-digit nanomolar range, except for **27** that displays the highest CB1R affinity of the series (K_i = 67.6 nM). The presence of the 3-methoxy group was also studied in the 2-benzyloxy analogue **13** (*i.e.,* the compound with the best compromise in terms of CB2R affinity and selectivity *vs* the CB1R). While the resulting di-functionalized compound **16** displays a lower CB2R affinity (K_i = 343.5 nM) compared to **13**, the interaction with the CB1R subtype is drastically reduced. Interestingly, **16** exhibits lower affinity than **19** and **29** suggesting that in the presence of the 3-methoxy group, a less bulky hydroxy or methoxy substituent in position 2 provides higher affinity towards CB2R. In order to interrogate other interaction-types with the CB2R binding site and in view of the polypharmacological action towards which these compounds are aimed (FAAH inhibition), the 5-position on the benzene ring (the other *meta* position to the carboxamide) was investigated by insertion of the bulky, electronegative bromine atom in the 2-hydroxy-3-methoxy, 2,3-dimethoxy and 2-benzyloxy-3-methoxy compounds (**12**, **23** and **24**, respectively). Curiously, the presence of the 5-bromo substituent is strongly detrimental in the absence of the 2-methoxy group, with **12** devoid of affinity and **24** displaying a 100-fold reduction in affinity (K_i = 3200 nM) compared to their not-brominated counterpart (**19** and **16**, respectively). By contrast, the dimethoxy derivative **23** retains CB2R affinity (K_i = 139.5 nM) just slightly lower than its corresponding not-brominated compound **29** (K_i = 87.6 nM). Notably, the presence of the 5-bromo substituent is able to recover a certain FAAH activity in the 2-hydroxy-3-methoxy and 2,3-dimethoxy derivatives compared to the not-brominated counterparts (as argued below). Except for **13**, **26** and **27**, displaying low CB1R affinity, all the compounds showed no interaction with the CB1R.

Table 1. In vitro Biological evaluation of the newly synthesized compounds.

Compound	R1	R2	R3	R4	CB2R K_i, nM ± SEM	CB1R, K_i, nM ± SEM or % @ 1μM[a]	FAAHi, IC$_{50}$ (μM)
9	H	H	H	H	NA	10	23.4±0.4
10	H	OCH$_3$	H	H	510±4.0	3	32.3±7.2
11	H	OCH$_3$	OCH$_3$	H	3000±289	4	>50
12	OH	OCH$_3$	H	Br	NA	3	38.4±1.2
13	OBz	H	H	H	14.8±4.49	241.3±2.4	4.0±2.3
14	H	OBz	H	H	313±41.7	19	24.1±1.9
15	H	H	OBz	H	3850±550	1	19.5±3.7
16	OBz	OCH$_3$	H	H	343.5±23.5	2	8.1±0.1
17	OH	H	H	H	NA	1	>50
18	H	H	OH	H	1060	4	>50
19	OH	OCH$_3$	H	H	153.1±25	2	>50
22	H	OH	H	H	NA	3	25.6±2.9
23	OCH$_3$	OCH$_3$	H	Br	139.5±33.50	6	44.6±3.9
24	OBz	OCH$_3$	H	Br	3200±1.6	3	8.8±1.0
25	OCH$_3$	H	H	H	387.4±10.4	5	48.5±8.8
26	OPentyl	H	H	H	10.8±1.9	152.9±22	6.2±1.4
27	OCH$_2$Cy	H	H	H	20.1±3.7	67.6±10.0	3.4±0.4
28	H	H	OCH$_3$	H	2450±220	2	>50
29	OCH$_3$	OCH$_3$	H	H	87.6±12	3	>50
GW405833					3.8±0.51		
Rimonabant						17.5	
JZL195							0.0196±0.003

[a]percentage of displacement at 1μM.

FAAH enzyme inhibition. As depicted in Table 1, Most of the compounds belonging to the series shows notable activity as FAAH inhibitors, covering three orders of magnitude (from low to high micromolar range). Remarkably, even the compounds whose IC$_{50}$ values are higher than 50 μM are still capable of slightly inhibiting the enzyme at that concentration (data not shown). More importantly, compared to the simplest compound in the series (**9**), it is clear that bulky, non-polar substituents in position 2 of the aromatic moiety, significantly increase (5-7-fold) the inhibitory activity towards FAAH (as seen for compounds **13**, **26** and **27**), while smaller or even polar

substituents such as hydroxyl or methoxy groups are disadvantageous (**17**, **25**). Similarly, except for compound **22**, small substituents in positions 3 or 4 of the benzene ring cause a decline of activity compared to the unsubstituted compounds (seen in **10**, but much sharper for **18**, **25** and **28**), while bulkier groups do not significantly impact on the inhibitory activity (**14**, **15**). As for **16**, the combination of a bulky substituent (benzyloxy) in position 2 and a methoxy in position 3 is only slightly disadvantageous, while the introduction of a bromine atom in position 5 (**24**) keeps the activity at FAAH unchanged. In contrast to this, combinations of small substituents, whether in position 2, 3 or 4, drastically reduce the potency of the compounds (**11**, **19**, **29**). The presence of a bromine atom in position 5, in this case, provides a slight recovery of potency (**12** and **23** compared to **19** and **29**, respectively). Notably, the same compounds that show the highest affinity for CB2R are also the best FAAH inhibitors (**13**, **26** and **27**). This is especially promising for the further development of novel multi-directed ligands active on these two pillars of the endocannabinoid system.

Functional Activity at CB2R in vitro. The three derivatives showing the best pharmacodynamic properties as dual agents (**13**, **26** and **27**), were tested to evaluate their CB2R functional profile. A CB2R-agonist action coupled with the inhibition of FAAH enzyme would synergize in the anti-inflammatory effect, thus leading to a potential neuroprotection. As above mentioned, this strategy could be also useful to stop the cytokines storm generated during the COVID-19, as well as during the first step in tumor onset (*i.e.* inflammation) or in neurodegeneration.

Therefore, the three compounds were tested in the cAMP assay showing a full agonist profile at CB2R in comparison with the reference compound JWH-133. As depicted in Table 2, a strict correlation between the CB2R affinity and CB2R activity was observed, with **26** displaying the best EC_{50} value (86.9 nM), followed by **13** (EC_{50}= 123.6 nM), and finally **27** (EC_{50}= 283.3 nM).

Table 2. Biological in vitro evaluation of CB2R activity.

compound	EC_{50}, nM	E_{MAX}, %
13	123.6	96.32
26	86.9	95.32
27	283.3	90.06
JWH-133	168.6	97.50

β2-arrestin recruitment assay. The concept of biased agonism has changed our comprehension of GPCR signaling, reshaping the preliminary optimization paradigm for GPCRs drug discovery.[34–41] Biased GPCR ligands can trigger a specific pathway responsible for a therapeutic effect, while not activating other signaling events eventually implicated in side effects. These ligands are valuable for clarifying key structural players in signal transduction pathways, besides their potential for developing therapeutic agents with fewer side effects. Thus, the early exploration of the functional signaling profile, mediated by G-protein on cAMP or β-arrestin, of the ligands under development is critical to define candidates.

It is well recognized that, β-arrestin-biased CB2R agonists, by increasing β2-arrestin recruitment, may induce receptor internalization and desensitization leading to decreased signaling and reduced receptor levels at the surface.[42] To further investigate the bias profile (e.g. balanced or biased) of

herein documented CB2R full agonists (**13**, **26** and **27**) we decided to explore their abilities to recruit β2-arrestin (Figure 3).

Table 3. β2-arrestin recruitment in vitro evaluation.

compound	EC_{50}, nM	E_{MAX}, %
13	51.82	12.6
26	23.85	34.5
27	10.73	5.5
CP55940	0.4	100
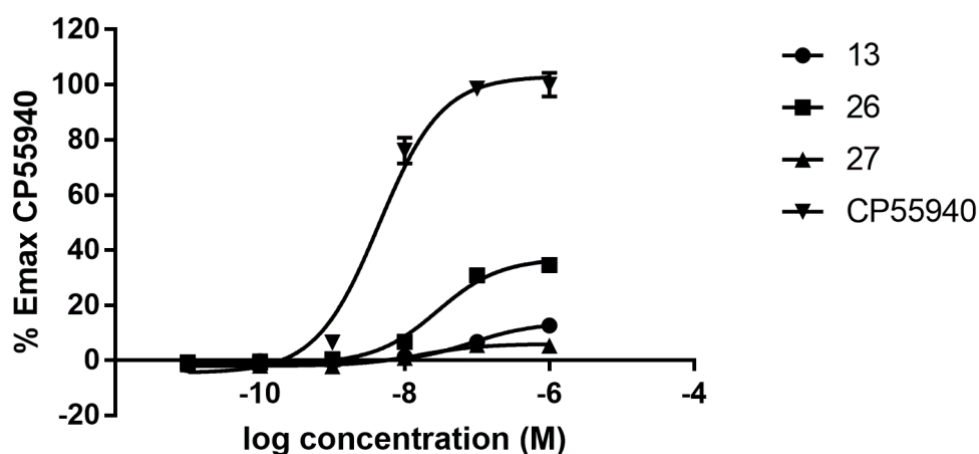
Figure 3. β2-arrestin recruitment dose-response curves.

The data indicates that all the compounds weakly recruit β2-arrestin in a concentration-dependent way, as weak partial agonists if we consider β-arrestin recruitment, being derivative **26** the one with the moderate efficacy (E_{max}= 34.5%), while the efficacy of **13** and **27** is almost negligible (E_{max}= 12.6%, 5.5%, respectively). All of them show EC_{50} values in the 2-digit nM range, being less active than CP55940 (subnanomolar EC_{50}) for activating this pathway (Figure 3, Table 3).

While more exhaustive studies are required, a comparative analysis of the EC_{50} values and efficacy at both signaling pathways suggest that the herein reported benzamides (**13**, **26** and **27**) behave as G-protein biased ligands.

Anti-inflammatory and pro-inflammatory cytokines production. The derivatives showing the best pharmacodynamic profile at the two desired targets, CB2R and FAAH, were tested for their ability

to modulate pro- and anti-inflammatory cytokines production in human monocytes and macrophages, where CB2R are present,[43–47] to have a picture of the impact of our compounds on circulating leukocytes (monocytes) or tissue-residing cells (macrophages). To simulate an inflammatory situation, we treated both monocytes and macrophages also with LPS, in order to evaluate the anti-inflammatory capabilities of these agents, in resting and activated leukocytes. We also tested the FAAH inhibitor reference compound JZL195 at its IC_{50} (20 nM), the CB2R reference agonist CB65[48] and the three CB2R full agonists **13**, **26** and **27** at 10 μM, alone and in the presence of the CB2R reference antagonist JTE907[49] 10 μM, in order to define the CB2R-mediated effect. The selected concentrations were chosen by preliminary dose-dependent assays (data not shown) where we found that CB65 and JTE907 at 10 μM reached the maximum effect, and the three compounds **13**, **26** and **27** exerted both their effects as FAAH inhibitors and CB2R agonists, considering their EC_{50}.

As depicted in Figure 4A and 4C, in unstimulated monocytes and macrophages, **13**, **26** and **27** decreased the pro-inflammatory cytokines TNFα, IFN-γ, IL-1β, IL6 production with efficacy comparable to the CB2R reference agonist CB65. Consistently, the compounds increased the anti-inflammatory cytokines IL-4 and IL-10 production along with reference compound CB65 (Figure 4A). The same variations in cytokine productions, although with a progressively greater extent, were detected in LPS-activated monocytes (Figure 4B) and macrophages (Figure 4D). As expected, the effect on cytokine production was significantly reversed by the CB2R antagonist JTE907 in all conditions. A few exceptions were observed where this trend was not statistically significant [i.e. reduction of IL-1β and IL-6 in basal monocytes for compound **26** (Figure 4A), reduction of IL-6 in LPS-activated monocytes for compounds **27** and **CB65** (Figure 4B), reduction of IL-6 for compound **13** or **CB65** along with increase of IL-10 for **CB65** in basal macrophages (Figure 4C), increase of IL-10 and IL-4 in LPS-activated macrophages for compound **13** (Figure 4D)]. Moreover, when compared with the effect of FAAH inhibitor JZL195, the efficacy of the agonists (**13**, **26**, **27**, **CB65**) in modulating cytokine release appeared to be generally greater (Figure 4A-4D) suggesting that the dual-targeting is indeed more beneficial than the mere CB2R activation or FAAH inhibition.

Overall, these results indicate that the three CB2R agonists **13**, **26** and **27** act as anti-inflammatory agents. It is interesting to note that the maximal reduction in pro-inflammatory cytokines and increase in anti-inflammatory cytokines have been detected in LPS-stimulated cells. These results suggest that our compounds are promising in counteracting situation of strong inflammation, both in circulating cells (e.g. in case of systemic infections or sepsis) and in tissue-residing cells. The latter observation sheds light on the possible exploitation of **13**, **26** and **27** as lead compounds for the development of drugs to be used in neuroinflammation, cancer or even to prevent the so-called "cytokine storm" associated to specific infective diseases, such as COVID-19.

THP1 monocytes (Basal) (A)

THP1 monocytes (LPS) (B)

THP1 macrophages (Basal) (C)
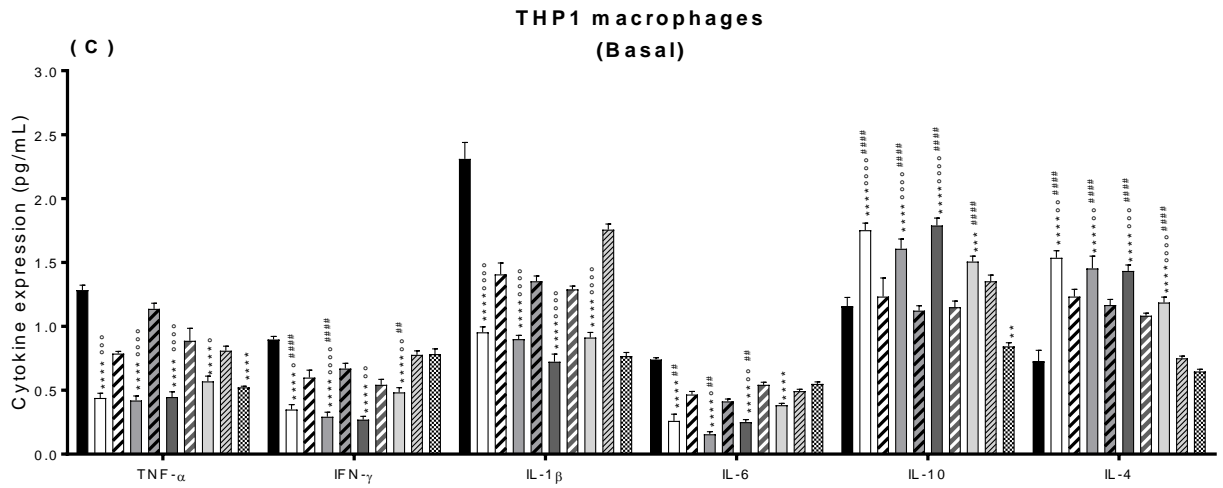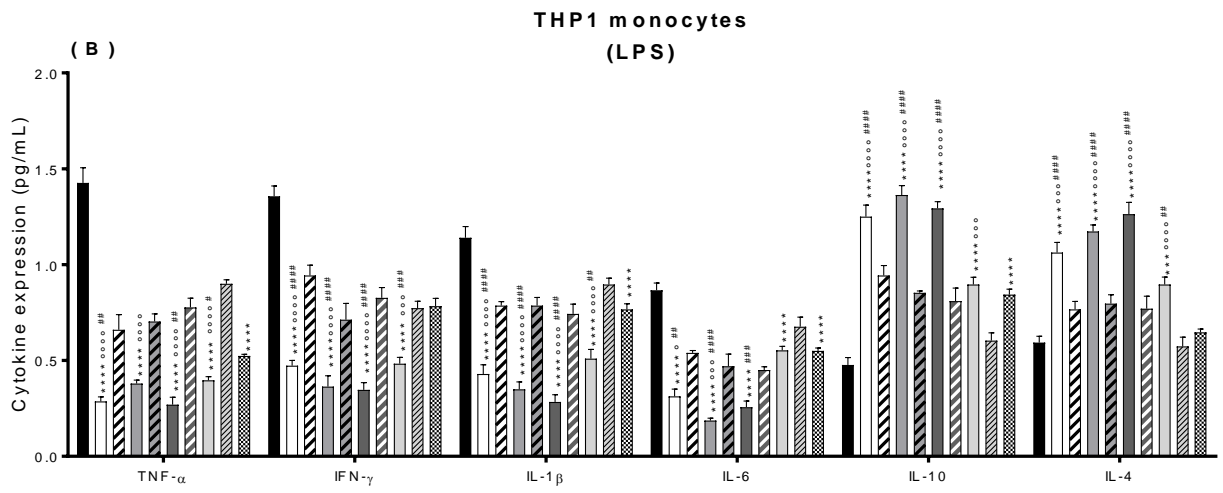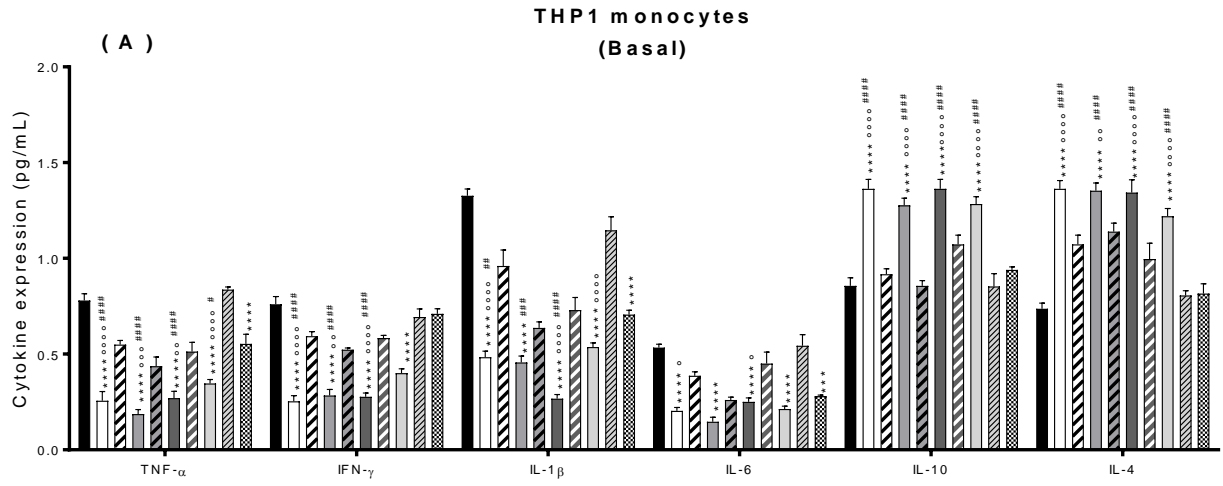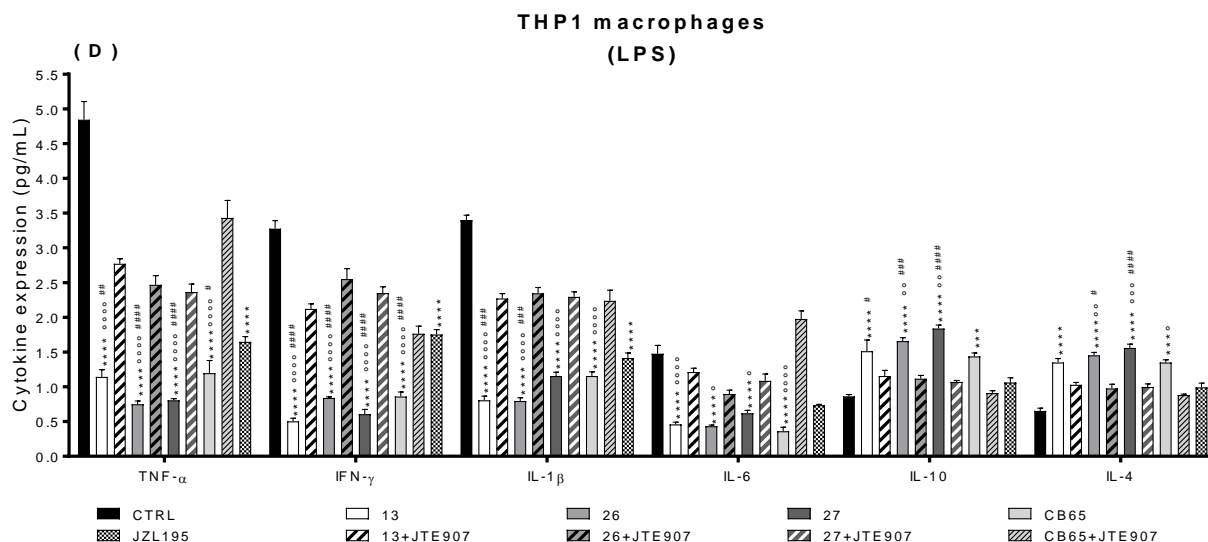
Figure 4. Cytokines levels in human monocytes and macrophages treated with CB2R/FAAH ligands. THP-1 cells, treated (C-D) or not (A-B) with 0.01 µM phorbol-12-myristate-13-acetate (PMA) for 48 h to differentiate them into macrophages, were incubated for additional 24 h in the absence (A, C) or presence of 10 µg/ml LPS (B, D), without (CTRL) or with the CB2R/FAAH ligands **13**, **26** and **27**, the CB2R agonist CB65 and the FAAH inhibitor JZL195. Compounds CB65, **13**, **26** and **27** were tested alone and in the presence of the CB2R inverse agonist JTE907. Cytokines levels were measured with an ELISA coupled with qRT-PCR. Data are means + SD (n=3). Two-Way ANOVA followed by Tukey post-hoc test was applied. Significance of symbols as follows: 1 symbol=p<0.05; 2 symbols= p<0.01; 3 symbols =p<0.001; 4 symbols=p<0.0001. Legend for symbols as follows: * indicates *vs* CTR;°indicates *vs* JTE907 in co-administration; # indicates *vs* JZL.

Functional Activity at CB1R in vitro. The residual affinity observed for **13**, **26** and **27** at CB1R (typically 3- to 20-fold lower than the affinity at CB2R) prompted us to investigate the functional activity of the three compounds at the CB1R, as well. The obtained data confirmed that all compounds behaved as full agonists, exhibiting modest (three-digit nanomolar) activity at CB1R (Table 4) compared to the reference compound **CP55940** (subnanomolar range). Comparison of CB2R and CB1R functional data confirms that the compounds described here show moderate selectivity for CB2R (Table 2) in agreement with the observed trend during the binding experiments (Table 1).

Table 4. Biological in vitro evaluation of CB1R activity.

compound	EC$_{50}$, nM	E_{MAX}, %
13	489	100
26	105.7	100
27	252.9	75
CP55940	0.2	100

Ferrozine-based assay. Salicylamides, as well as benzamides, are able to chelate metals such as iron species and may thus be useful as scavengers of toxic metal ions.[25] Accordingly, we evaluated the ability of the amides herein reported to chelate iron(II) through the 'Ferrozine assay', that is the colorimetric assay used for the quantitation of iron(II) in cultured cells.[50]

All the newly synthesized compounds are able to compete with Ferrozine in chelating the ion to the same extent of salicylic acid (Figure S2), with a slightly higher activity shown by the two *o*-benzyloxy derivatives **13** and **24**. Interestingly, the presence of the *p*-hydroxy or *p*-methoxy (**18** and **28**) groups confers the highest potency. On the other hand, the *p*-benzyloxy substituent (**15**) does not confer this same property, with results comparable to the other amides.

The metal chelating ability of these multifunctional compounds supports their potential as neuroprotective agents since the metal toxicity is a hallmark in neurodegeneration triggering the oxidative stress.[51]

Molecular docking. As mentioned above, the 2-benzyloxy analog (**13**) is responsible for a higher CB2R affinity (K_i = 14.8 nM) compared to the 3- (**14**, K_i = 313 nM) and 4-substituted (**15**, K_i = 3850 nM). Aimed at getting molecular insights into the Structure Activity Relationships (SARs) occurring in our derivatives, we subjected these compounds to molecular docking simulations. More specifically, we employed, as starting protein structure, the recently published X-ray data of the CB2R receptor complexed with an agonist (PDB code: 6KPC, released in 2020[52]). **Figure 5** shows the obtained top-scored docking poses. It is worth noting that the derivatives are predicted to share the same binding mode based on ligand-protein shape complementarity. Remarkably, the computed MM-GBSA scores agree with the experimental data: the best one being that returned by compound **13** (-85.6 kcal/mol), followed by **14** (-80.8 kcal/mol), and **15** (-72.7 kcal/mol). In order to better rationalize these data, we performed an analysis of the single contributions responsible for the total MM-GBSA score. Remarkably, most of the computed binding energy is due to the presence of lipophilic interactions (shape complementarity) as testified by the corresponding *MM-GBSA lipo* contribution (53.6 kcal/mol, -52.0 kcal/mol and -52.7 kcal/mol for **13**, **14**, and **15** respectively). Remarkably, a difference contribution is instead observed in terms of van der walls (vdw) interactions, being the *MM-GBSA vdw* score equal to -59.2 kcal/mol for compound **13** and -50.94 kcal/mol and -46.64 kcal/mol for compounds **14** and **15**, respectively. Building on that, we performed an in-depth analysis of the obtained top-scored docking poses by performing a visual inspection and by generating the Structural Interaction Fingerprint (SIFt) that converts the 3D structural binding information into a one-dimensional (1D) binary string.[53,54] Remarkably, **13** is predicted to establish a total number of hydrophobic interactions (15) higher than **14** (12) and **15** (11). In particular, as shown in Figure 5A, **13** establishes a pi-pi interaction with F87 and several hydrophobic interactions involving F91, F117, V186, Y190, W258, and C288. The binding mode returned by **14** (Figure 5B) and **15** (Figure 5C) is quite similar to that of **13**, with a pi-pi interaction established with F117 and several hydrophobic interactions. However, it is worth noting that **14** does not make vdw contacts with I186, Y190, and C288; while **15** with F91, W258, and C288. Finally, to rationalize the significant increase in the CB2R affinity conferred by the 2-benzyloxy group if compared to the 2-methoxy one (**Table 1**), we performed molecular docking simulations of the derivative **25**. As shown in Figure 5D, the top-scored docking pose is quite similar to that of **13**, and, again, molecular recognition is predicted to be the consequence of several hydrophobic interactions involving F87, F91, F117, W258, and C288. However, **25** is predicted to establish less hydrophobic contacts with respect to **13** as a consequence of the different size of the substituent in position 2 (benzyloxy vs. methoxy). Consistently, the MM-GBSA score returned by **13** (-85.6 kcal/mol) is better than that computed for **25** (-63.6 kcal/mol). These results, taken together, put forward the adopted computational workflow as valuable for rationally explaining the importance of a bulky substituent in positions 2, rather than 3 and 4, to maximize the affinity towards CB2R. Encouraged by these data, we also performed molecular docking simulations of compounds **26** and **27**, being both characterized by bulky substituents in

position 2 and high affinities (K_i = 10.8 nM and 20.1 nM, respectively), as reported in Table 1. As expected, molecular recognition is again the result of a shape complementarity and an important role seems to be played by the hydrophobic interactions (with F91, Y190, W258, and C288). In addition, pi-pi interactions are predicted to be established with F87 (**26**) and F117 (**27**). Importantly, high binding free energies are computed for all the investigated ligands, being the computed MM-GBSA score of **26** and **27** equal to -76.5 kcal/mol (MM-GBSA lipo = -44.3 kcal/mol; MM-GBSA vdw = -50.1 kcal/mol) and - 75.7 kcal/mol (MM-GBSA lipo = -49.3 kcal/mol; MM-GBSA vdw = -51.5 kcal/mol), respectively.

For the sake of completeness, we also performed molecular docking simulations of **13**, **26**, and **27** within the binding site of CB1R by using the X-ray structure of the receptor complexed with an agonist (PDB code: 5XRA),[55] as the obtained experimental data indicate that these molecules act as CB1R weak agonists. Remarkably, the predicted binding mode for these ligands in the CB1R is quite similar to that of CB2R. Compounds **13**, **26**, and **27** share several hydrophobic interactions involving F189, F268, L276, F174, and L359 and good MM-GBSA scores (see supporting information).

Finally, to provide a rationale, from a molecular point of view, behind the observed dual FAAH/CB2R activities, we performed molecular docking simulations within the binding sites of FAAH. As mentioned above, the obtained experimental data suggest that the investigated molecules act as CB2R agonists and FAAH non-covalent inhibitors. As far as the FAAH enzyme is concerned, a 3D structure of the human form is not available in the Protein Data Bank. However, as recently pointed out by Mileni *et al*,[56] the release of human (h) /rat (r) engineered FAAH structures allows for the investigation of the interactions occurring between covalent or non-covalent inhibitors and the binding site of the human form with good approximation. We therefore performed docking simulations on the X-ray structure released in 2018 by Seierstad et al., showing the h/r FAAH in complex with the non-covalent inhibitor JXV (PDB code: 6MRG).[57] More specifically, we focused our attention on three compounds belonging to our series, **13**, **26** and **27**, namely the derivatives of our panel displaying micromolar activity towards FAAH and nanomolar affinity at CB2R (**Table 1**). **Figure 6** shows the obtained top-scored docking poses returned by these three ligands within the employed FAAH crystal structure. It is worth noting that the binding mode returned by the ligands (based on the inspection of the employed x-ray data) is almost the same and reproduces the mode experimentally observed for the co-crystallized ligand JXV.

As in Figure 6, molecular recognition is the result of an effective shape complementarity between the investigated ligands and the FAAH binding site. More specifically, several hydrophobic interactions involving L404, I407, L429, L433, V491, and M495 are observed in all the top-scored docking poses. The importance of these interactions is supported by the evidence that the main contributions to the computed MM-GBSA scores are those returned by the terms named MM-GBSA lipo (lipophilic binding energy) and MM-GBSA vdw (Van der Waals binding energy). Remarkably, in agreement with the experimental data, the best MM-GBSA score (-66.5 kcal/mol) is returned by **27** (MM-GBSA lipo = -38.4 kcal/mol; MM-GBSA vdw = -55.9 kcal/mol) while MM-GBSA score equal to -55.9 kcal/mol (MM-GBSA lipo = -36.1 kcal/mol, MM-GBSA vdw = -46.6 kcal/mol) and - 60.68 kcal/mol (MM-GBSA lipo = -36.4 kcal/mol; MM-GBSA vdw = -50.7 kcal/mol) were obtained by **13** and **26**, respectively. These results, taken together, put forward the adopted computational workflow as valuable for rationally designing lipophilic molecules able to act, at the same time, as non-covalent FAAH inhibitors and CB2R agonists.
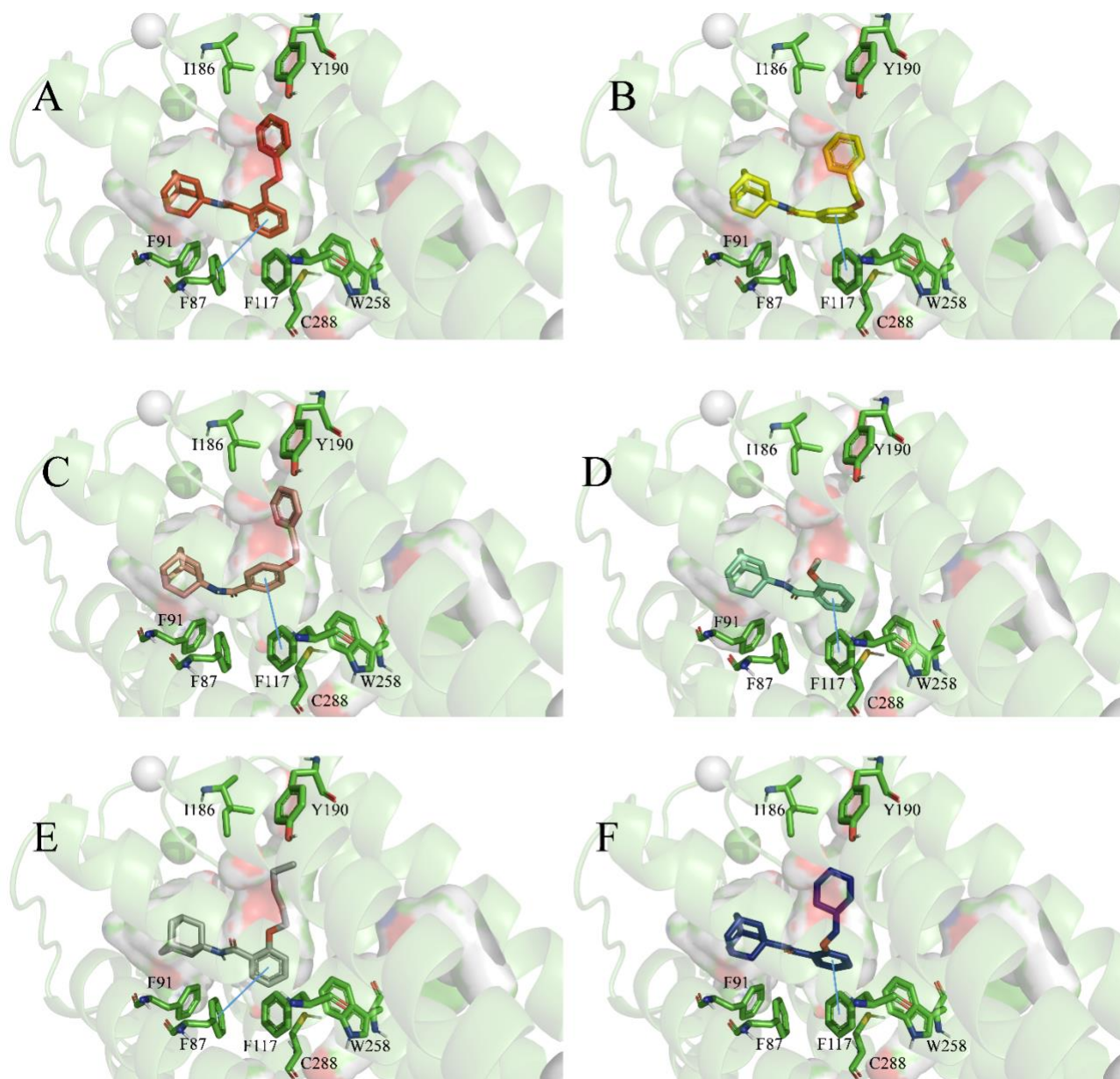
Figure 5. Top-scored docking poses returned by docking simulations performed on **13** (A), **14** (B), **15** (C), **25** (D), **26** (E) and **27** (F) within the binding site of CB2R (PDB code: 6KPC). Ligands and important residues are rendered as sticks, the protein as cartoon and its binding pocket as surface. The pi-pi interactions are itemized by a blue line. For the sake of clarity, only polar hydrogen atoms are shown.
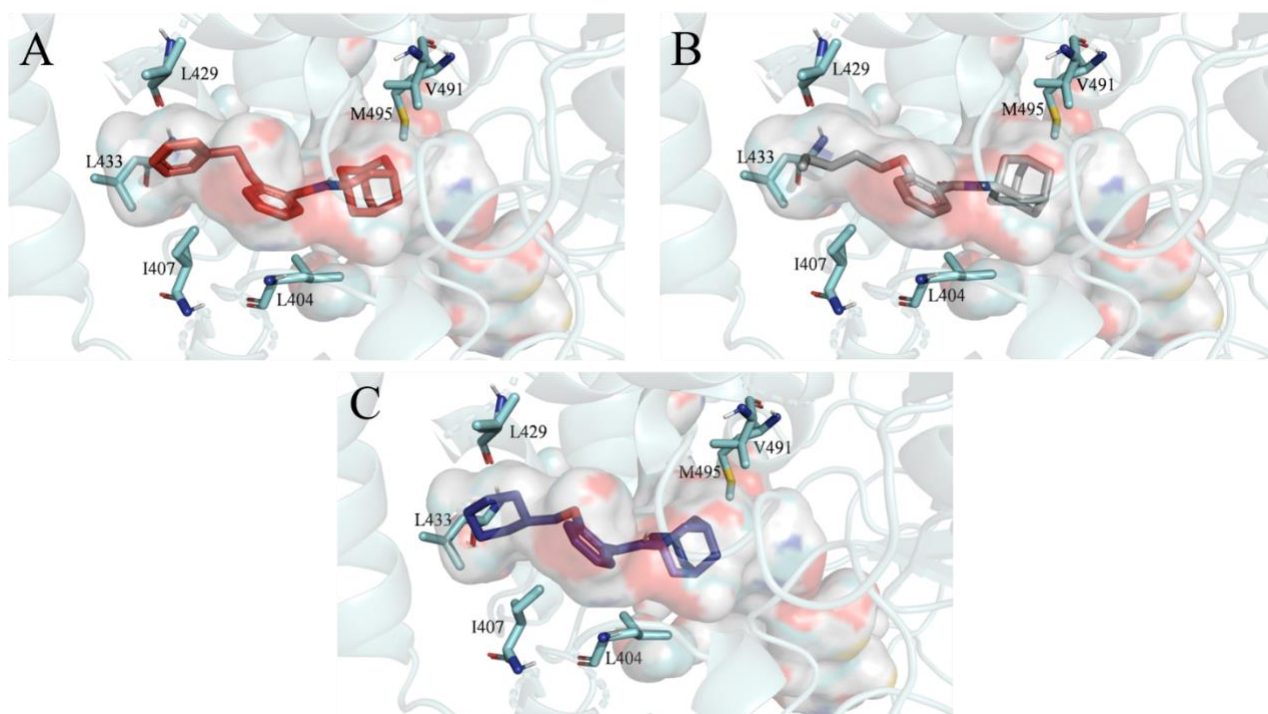
Figure 6. Top-scored docking poses returned by docking simulations performed on **13** (A), **26** (B) and **27** (C) within the binding site of FAAH (PDB code: 6MRG). Ligands and important residues are rendered as sticks, the protein as cartoon and its binding pocket as surface. For the sake of clarity, only polar hydrogen atoms are shown.

CONCLUSIONS

In the frame of a program to identify novel multitarget agents, able to face diseases characterized by early and significant inflammatory cascades (e.g., neurodegeneration, cancer, and COVID-19), herein we proposed and validated the potential of a novel approach based on dual ligands targeting CB2R and FAAH. Inspired by previous SAR and SAfiR studies and the study of common diversity space (PCA) of ligands for these targets, we conceived and obtained novel series of *N*-adamantyl benzamides as dual CB2R agonists and FAAH inhibitors. The pharmacodynamic profile (CB2R affinity and selectivity as well as the ability to inhibit the FAAH enzyme) of the scaffold was optimized by modifying the substitution pattern at the aromatic core of the *N*-adamantyl benzamides. Three derivatives (**13**, **26** and **27**), exhibiting excellent CB2R affinity and moderate FAAH inhibitory activity, emerged as attractive multitarget agents and were selected for functional experiments and computational studies to rationalize the experienced bioactivity from a molecular modeling perspective. Functional studies evidenced that selected compounds are full agonists at CB2R, with preliminary data suggesting a G-protein biased behavior. Importantly, the selected compounds were proved to reduce in a statistically significant manner the pro-inflammatory cytokines production and at the same time to induce the anti-inflammatory ones in macrophages and monocytes, mainly in the inflammatory-activated state. This effect was not totally reverted by the CB2R inverse agonist JTE907, suggesting a contribution probably due to the FAAH inhibition, although off-target effects may also be considered. Indeed, the best compounds **13**, **26** and **27** are also endowed with a CB1R agonist activity, although much weaker than the reference compound. Additionally, these novel molecules were found to be able to overcome BBB and proved to be iron(II) species chelators, suggesting their potential ability as metal scavengers, in diseases also characterized by unbalanced

metal levels. Based on the data presented herein, the *N*-adamantyl benzamides **13**, **26** and **27** may be considered as lead compounds for the development of new agents able to prevent the detrimental inflammatory cascade occurring in severe neurodegenerative diseases (i.e. AD), in the cancer onset and progression and also in the COVID-19 infection.

EXPERIMENTAL SECTION

Principal component analysis. 4,551 activity entries were extracted from ChEMBL v30 according to the ID assigned to the CB2R (1,827 entries - CHEMBL253) and FAAH (2724 entries - CHEMBL2243) targets. In particular, to ensure data validity[54] only those entries matching the following criteria were considered: i) annotations with IC_{50} and k_i measures, *ii*) assays conducted on human targets ("target_organism" = "Homo sapiens") and marked as direct binding ("assay_type" = "B"), and *iii*) entries free of warnings in the "data_validity_comment" field. The retrieved SMILES were curated using the Speedy SMILES nodes, available in KNIME and developed by Vernalis Research,[58] to neutralize salts and remove organometallic and inorganic compounds. Subsequently, these SMILES were converted to a canonical format using Openbabel.[59] After duplicates removal, we retained only those compounds displaying an IC_{50} (or k_i) ≤ 1 µM. In doing that, we finally selected 1020 (CB2R) and 406 (FAAH) binders. 16 physicochemical descriptors were computed and standardized for each ligand using the CDK toolkit[60] and the Normalizer KNIME node.[58,61] Finally, a PCA allowed simplifying the high dimensionality resulting from the computed descriptors to two principal components (able to explain 70 % of the computed variance) and, therefore, plotting each ligand within a 2D chemical space (Figure 1).

Chemistry. All chemicals, unless otherwise stated, were purchased from Sigma-Aldrich, TCI Chemicals, Alfa Aesar, or Acros Organics. Thin layer chromatography (TLC) was performed using plates from Merck (silica gel 60 F254). Column chromatography was performed with Merck silica gel 60 Å (63-200 mm) as the stationary phase. Melting points were determined in open capillaries on a Gallenkamp electrothermal apparatus. ^{1}H-NMR spectra were recorded in the indicated solvent on a Varian Mercury-VX spectrometer (300 MHz) or on an Agilent 500-vnmrs500 spectrometer (499.801 MHz). The following data are reported: chemical shift (δ) in ppm, multiplicity (s = singlet, d = doublet, t = triplet, dd = doublet of doublets, dt = doublet of triplets m = multiplet, br = broad signal), integration, and coupling constant (*J*) in hertz. Recording of mass spectra was done on an HP6890-5973 MSD gas chromatograph/mass spectrometer; only significant *m/z* peaks, with their percentage of relative intensity in parentheses, are reported. HRMS-ESI analyses were performed on a Bruker Daltonics MicrOTOF-Q II mass spectrometer. All spectra were in accordance with the assigned structures. The purity of target compounds was assessed by HPLC. Analytical HPLC analyses were performed on a Shimadzu Prominance Modular HPLC equipped with a diode array detector (DAD) using a reversed phase column (Shim-pack VP-ODS C18 250 mm x 4.6 mm, 5 µ). Isocratic elution was conducted at a flow rate of 1 mL/min with CH_3OH/H_2O (80:20, v/v). UV signal was detected at 254 nm, 280 nm, and 320 nm. Purity for all compounds is > 95% by HPLC.

General procedure for the synthesis of adamantyl-amides (**9-16**), (**21**). The appropriate carboxylic acid among **1-8** and **20** (0.87 mmol, 0.2 g) was dissolved in dry DMF (4 mL). The solution was cooled at 0° C and DIPEA (2.6 mmol, 0.5 mL) was added under argon atmosphere and stirred for 10 min. HBTU (1.31 mmol, 0.5 g) was then added to the solution and the reaction mixture was stirred under argon atmosphere at room temperature for 2 h. 1-Adamantanamine (1.31 mmol, 0.2 g) was added to the solution and the mixture was stirred at room temperature for 18 h under argon. The reaction mixture was then poured into H_2O (20 mL) and extracted with CH_2Cl_2 (3 × 20 mL). The collected

organic layers were washed with HCl 1N (20 mL), H_2O (20 mL), and brine (3 × 20 mL), dried over Na_2SO_4, and concentrated under vacuum. The crude product was purified by column chromatography (1:30) using CH_2Cl_2/AcOEt (9:1) as eluent to afford the appropriate adamantylamide.

N-(Adamantan-1-yl)benzamide (**9**). The title compound was obtained as a white solid with a quantitative yield; mp, 153-155 °C. ^{1}H-NMR (300 MHz, CDCl$_3$) δ: 1.67-1.73 (m, 6H), 2.11-2.12 (m, 9H), 5.86 (br s, 1H), 7.36 (t, 2H, *J* = 6.8 Hz, aromatic), 7.41-7.44 (m, 1H, aromatic), 7.69 (d, 2H, *J* = 6.8 Hz, aromatic). HRMS-ESI for C$_{17}$H$_{21}$NO (*m/z*): [M+Na]$^+$ calcd, 278.1525; found, 278.1524; [2M+Na]$^+$ calcd, 533.3139; found, 533.3156.

N-(Adamantan-1-yl)-3-methoxybenzamide (**10**). The title compound was obtained as a brown solid with a 44 % yield; mp, 127-129 °C. ^{1}H-NMR (300 MHz, CDCl$_3$) δ: 1.65-1.74 (m, 6H), 2.10-2.12 (m, 9H), 3.80 (s, 3H), 5.85 (br s, 1H), 6.94-6.99 (m, 2H, aromatic), 7.21-7.31 (m, 2H, aromatic). HRMS-ESI for C$_{18}$H$_{23}$NO$_2$ (*m/z*): [M+Na]$^+$ calcd, 308.1621; found, 308.1638; [2M+Na]$^+$ calcd, 593.3350; found, 593.3382.

N-(Adamantan-1-yl)-3,4-dimethoxybenzamide (**11**). The title compound was obtained as a white solid with a 30 % yield; mp, 195-197 °C. ^{1}H-NMR (300 MHz, CDCl$_3$) *δ*: 1.62-1.71 (m, 6H), 2.04-2.08 (m, 9H), 3.85 (s, 3H), 3.86 (s, 3H), 5.83 (br s, 1H), 7.28 (d, 1H, *J* = 6.7 Hz, aromatic), 7.14-7.17 (m, 1H, aromatic), 7.36 (d, 1H, *J* = 7.8 Hz, aromatic). HRMS-ESI for C$_{19}$H$_{25}$NO$_3$ (*m/z*): [M+Na]$^+$ calcd, 338.1727; found, 338.1731; [2M+Na]$^+$ calcd, 653.3572; found, 653.3571.

N-(Adamantan-1-yl)-5-bromo-2-hydroxy-3-methoxybenzamide (**12**). The title compound was obtained as a pink solid with a 31 % yield; mp, 242-243 °C. ^{1}H-NMR (300 MHz, CDCl$_3$) *δ*: 1.68-1.72 (m, 6H), 2.11-2.13 (m, 9H), 3.87 (s, 3H), 5.99 (br s, 1H), 7.02-7.06 (m, 2H, aromatic), 7.25 (br s, 1H). HRMS-ESI for C$_{18}$H$_{22}$NO$_3$Br (*m/z*): [M-H]$^-$ calcd, 378.0707; found, 378.0705.

N-(Adamantan-1-yl)-2-(benzyloxy)benzamide (**13**). The title compound was obtained as a brown crystal with a 97% yield; mp, 135-138 °C. ^{1}H-NMR (300 MHz, CDCl$_3$) *δ*: 1.63-1.68 (m, 6H), 1.85-1.90 (m, 6H), 1.97-1.98 (m, 3H), 5.11 (s, 2H), 7.02-7.08 (m, 3H, aromatic), 7.36-7.48 (m, 5H, aromatic), 7.69 (br s, 1H), 8.17 (dd, 1H, *J$_1$* = 6.8 Hz, *J$_2$* = 3.5 Hz, aromatic). HRMS-ESI for C$_{24}$H$_{27}$NO$_2$ (*m/z*): [M+Na]$^+$ calcd, 384.1934; found, 384.1944; [2M+Na]$^+$ calcd, 745.3976; found, 745.3994; [M+H]$^+$ calcd, 362.2121; found, 362.2115.

N-(Adamantan-1-yl)-3-(benzyloxy)benzamide (**14**). The title compound was obtained as a white crystal with a 48 % yield; mp, 148-149 °C. ^{1}H-NMR (300 MHz, CDCl$_3$) *δ*: 1.68-1.76 (m, 6H), 2.11-2.12 (m, 9H), 5.10 (s, 2H), 7.05-7.09 (m, 1H, aromatic), 7.23-7.45 (m, 9H, aromatic + NH). HRMS-ESI for C$_{24}$H$_{27}$NO$_2$ (*m/z*): [M+Na]$^+$ calcd, 384.1934; found, 384.1939.

N-(Adamantan-1-yl)-4-(benzyloxy)benzamide (**15**). The title compound was obtained as a brown crystal with a 63 % yield; mp, 151-153 °C. ^{1}H-NMR (300 MHz, CDCl$_3$) *δ*: 1.67-1.76 (m, 6H), 2.05-2.16 (m, 9H), 5.10 (s, 2H), 5.72 (br s, 1H), 6.94-6.99 (m, 2H, aromatic), 7.31-7.44 (m, 5H, aromatic), 7.65-7.70 (m, 2H, aromatic). HRMS-ESI for C$_{24}$H$_{27}$NO$_2$ (*m/z*): [M+H]$^+$ calcd, 384.1934; found, 384.1938; [2M+Na]$^+$ calcd, 745.3976; found, 745.3988.

N-(Adamantan-2-(benzyloxy)-3-methoxy benzamide (**16**). The title compound was obtained as an orange solid with a 50 % yield; mp, 90-92 °C. ^{1}H-NMR (500 MHz, CDCl$_3$) *δ*: 1.62-165 (m, 6H), 1.85-1.87 (m, 6H), 1.99-2.02 (m, 3H), 3.92 (s, 3H), 5.06 (s, 2H), 7.07 (d, 1H, *J* = 8.1 Hz, aromatic), 7.14-7.18 (m, 1H, aromatic), 7.36-7.43 (m, 4H, aromatic), 7.67-7.69 (m, 1H, aromatic), 7.72 (br s, 1H). HRMS-ESI for C$_{25}$H$_{29}$NO$_3$ (*m/z*): [M+Na]$^+$ calcd, 414.2040; found, 414.2029; [2M+Na]$^+$ calcd, 805.4188; found, 805.4215.

3-(Adamantan-1-yl-carbamoyl)phenyl acetate (**21**). The title compound was obtained as a white solid with a 45 % yield; mp, 111-112 °C. ^{1}H-NMR (300 MHz, CDCl$_3$) δ: 1.62-1.66 (m, 6H), 2.05-2.08 (m, 9H), 2.24 (s, 3H), 5.91 (br s, 1H), 7.10-7.14 (m, 1H, aromatic), 7.30-7.36 (m, 1H, aromatic), 7.40 (t, 1H, $J = 6$ Hz, aromatic), 7.50-7.53 (m, 1H, aromatic). HRMS-ESI for C$_{18}$H$_{23}$NO$_3$ (*m/z*): [M+H]$^+$ calcd, 336.1576; found, 336.1568; [2M+Na]$^+$ calcd, 649.3254; found, 649.3236.

General procedure for the debenzilation of N-Adamantanyl(benzyloxy)benzamide for the synthesis of final compounds 17-19. The appropriate benzyloxy derivate among **13**, **15** or **16** (0.27 mmol, 0.1 g) was dissolved in MeOH (10 mL) and added with Pd on carbon 10% (0.03 g). The mixture was hydrogenated at a H$_2$ pressure of 2.5 bar at room temperature for 48 h upon stirring. The reaction was filtered on Celite and washed with MeOH. The solvent was removed by rotary evaporation affording the title compound that was not further purified.

N-(Adamantan-1-yl)-2-hydroxybenzamide (**17**). The title compound was obtained as a white solid with a 99 % yield; mp, 162-164 °C. ^{1}H-NMR (300 MHz, DMSO-d$_6$) δ: 1.52-1.60 (m, 6H), 2.48-2.49 (m, 9H), 5.73 (br s, 1H), 6.53 (t, 1H, $J = 6$ Hz, aromatic), 6.71 (d, 1H, $J = 6$ Hz, aromatic), 7.11 (t, 1H, $J = 6$ Hz, aromatic), 7.75 (dd, 1H, $J_1 = 6$ Hz, $J_2 = 1.5$ Hz, aromatic), 9.69 (br s, 1H). HRMS-ESI for C$_{17}$H$_{21}$NO$_2$ (*m/z*): [M-H]$^-$ calcd, 270.1495; found, 270.1498.

N-(Adamantan-1-yl)-4-hydroxybenzamide (**18**). The title compound was obtained as a white solid with a 76 % yield; mp, 220-222 °C. ^{1}H-NMR (300 MHz, CD$_3$OD) δ: 1.73-1.78 (m, 6H), 2.09-2.14 (m, 9H), 6.77 (d, 2H, $J = 6$ Hz, aromatic), 7.60 (d, 2H, $J = 6$ Hz, aromatic). HRMS-ESI for C$_{17}$H$_{21}$NO$_2$ (m/z): [M-H]$^-$ calcd, 270.1495; found, 270.1499.

N-(Adamantan-1-yl)-2-hydroxy-3-methoxybenzoic acid (**19**). The title compound was obtained as a pink solid with a 45 % yield; mp, 124-126 °C. ^{1}H-NMR (300 MHz, CDCl$_3$) δ: 1.67-1.72 (m, 6H), 2.12-2.16 (m, 9H), 3.88 (s, 3H), 6.09 (br s, 1H), 6.71-6.80 (m, 1H, aromatic), 6.94 (d, 2H, $J = 8.0$ Hz, aromatic), 12.35 (br s, 1H). HRMS-ESI for C$_{18}$H$_{23}$NO$_3$ (*m/z*): [M-H]$^-$ calcd, 301.1601; found, 301.1603.

N-(Adamantan-1-yl)-3-hydroxybenzamide (**22**). The acetylated derivative **21** (3.72 mmol, 1.164 g) was dissolved in a mixture 2:1 of MeOH (20 mL) and H$_2$O (10 mL). NaHCO$_3$ (5.2 mmol, 0.437 g) was added and the reaction mixture was stirred at room temperature for 2 h. The solution was acidified (HCl 2N) and extracted with CH$_2$Cl$_2$ (3 × 20 mL). The organic layers were dried over Na$_2$SO$_4$ and concentrated under vacuum to afford the crude product. Purification by column chromatography (1:30) using CH$_2$Cl$_2$/AcOEt (9:1) as eluent afforded **22** as a white solid with a 80 % yield; mp, 211-213 °C. ^{1}H-NMR (300 MHz, CD$_3$OD) δ: 1.74-1.76 (m, 6H), 2.09-2.11 (m, 9H), 5.48 (br s, 1H), 6.87-6.91 (m, 1H, aromatic), 7.11-7.14 (m, 1H, aromatic), 7.16-7.17 (m, 1H, aromatic), 7.19-7.21 (m, 1H, aromatic), 7.24 (br s, 1H).

General procedure for the alkylation of hydroxybenzamides for the synthesis of final amides 23-29.

The appropriate hydroxybenzamide among **12**, **17-19** (0.52 mmol, 0.142 g) was solubilized in acetone (30 mL). The appropriate alkyl halide (1.56 mmol,) and K$_2$CO$_3$ (1.57 mmol, 0.22 g) were added. The reaction was carried out under reflux for 4 h upon stirring. The solvent was evaporated under reduced pressure, the crude was taken up with water (15 mL) and extracted with CH$_2$Cl$_2$ (3 × 15 mL). The combined organic layers were dried on Na$_2$SO$_4$ and concentrated under vacuum. The crude product was purified by column chromatography (1:30) using CH$_2$Cl$_2$/AcOEt (9:1) as eluent to afford the title compound.

N-(Adamantan-1-yl)-5-bromo-2,3-dimethoxybenzamide (**23**). Iodomethane (0.76 mmol, 0.037 g) was used for the methylation of compound **12**. The title compound was obtained as a white solid with a 79 % yield; mp, 74-76 °C. ^{1}H-NMR (300 MHz, CDCl$_3$) δ: 1.69-1.75 (m, 6H), 2.10-2.12 (m, 9H), 3.84 (s, 3H), 3.86 (s, 3H), 7.11 (d, 1H, J = 1.5 Hz, aromatic), 7.67 (br s, 1H), 7.76 (d, 1H, J = 1.5 Hz, aromatic). HRMS-ESI for C$_{19}$H$_{24}$BrNO$_3$ (*m/z*): [M+Na]$^+$ calcd, 418.0812; found, 418.0812; [2M+Na]$^+$ calcd, 811.1751; found, 811.1766.

N-(Adamantan-1-yl)-2-(benzyloxy)-5-bromo-3-methoxybenzamide (**24**). Bromomethylbenzene (0.288 mmol, 0.034 mL) was used for the alkylation of compound **12**. The title compound was obtained as a pink solid with a 71 % yield; mp, 117-119 °C. ^{1}H-NMR (300 MHz, CDCl$_3$) δ: 1.59-1.64 (m, 6H), 1.81-1.84 (m, 6H), 1.98-2.03 (m, 3H), 3.90 (s, 3H), 5.03 (s, 2H), 7.13 (d, 1H, J = 1.5 Hz, aromatic), 7.40-7.44 (m, 5H, aromatic), 7.58 (br s, 1H), 7.79 (d, 1H, J = 1.5 Hz, aromatic). HRMS-ESI for C$_{25}$H$_{28}$BrNO$_3$ (*m/z*): [M+Na]$^+$ calcd, 494.1125; found, 494.1129; [2M+Na]$^+$ calcd, 963.2377; found, 963.2389.

N-(Adamantan-1-yl)-2-methoxybenzamide (**25**). Iodomethane (0.39 mmol, 0.056 g) was used for the methylation of compound **17**. The title compound was obtained as a white solid with a 67 % yield; mp, 158-160 °C. ^{1}H-NMR (300 MHz, CDCl$_3$) δ: 1.65-1.75 (m, 6H), 2.10-2.13 (m, 9H), 3.92 (s, 3H), 6.93 (d, 1H, J = 9 Hz, aromatic), 7.06 (t, 1H, J = 8.5 Hz, aromatic), 7.40 (dt, 1H, J_1 = 9 Hz, J_2 = 1.2 Hz, aromatic), 7.69 (br s, 1H), 8.14 (dd, 1H, J_1 = 8 Hz, J_2 = 1.2 Hz, aromatic). HRMS-ESI for C$_{18}$H$_{23}$NO$_2$ (*m/z*): [M+Na]$^+$ calcd, 308.1621; found, 308.1626; [2M+Na]$^+$ calcd, 593.3350; found, 593.3362.

N-(Adamantan-1-yl)-2-(pentyloxy)benzamide (**26**). 1-Bromopentane (0.288 mmol, 0.043 g) was used for the alkylation of compound **17**. The title compound was obtained as a white solid with a 35% yield; mp, 82-84 °C. ^{1}H-NMR (300 MHz, CDCl$_3$) δ: 0.96 (t, J = 7.2 Hz, 3H), 1.42-1.47 (m, 2H), 1.49-1.55 (m, 2H), 1.73-1.81 (m, 6H), 1.82-1.91 (m, 2H), 2.12-2.14 (m, 9H), 4.09 (t, J = 6.4 Hz, 2H), 6.91 (d, 1H, J = 6 Hz, aromatic), 7.05 (t, 1H, J = 6 Hz, aromatic), 7.37 (t, 1H, J = 6 H, aromatic), 7.90 (br s, 1H), 8.16 (dd, 1H, J_1 = 6 Hz, J_2 = 1 Hz, aromatic). HRMS-ESI for C$_{22}$H$_{31}$NO$_2$ (*m/z*): [M+Na]$^+$ calcd, 364.2247; found, 364.2253; [2M+Na]$^+$ calcd, 705.4602; found, 705.4622.

N-(Adamantan-1-yl)-2-cyclohexylmethoxy-benzamide (**27**). Bromomethyl cyclohexane (1.56 mmol, 0.278 g) was used for the alkylation of compound **17**. The title compound was obtained as white crystal with a 25% yield; mp, 134-136 °C. ^{1}H-NMR (500 MHz, CDCl$_3$) δ: 1.05-1.13 (m, 2H), 1.19-1.35 (m, 3H), 1.65-1.68 (m, 6H), 1.71-1.74 (m, 4H), 1.78- 1.88 (m, 2H), 2.03-2.12 (m, 9H), 3.86-3.87 (m, 2H), 6.89 (d, 1H, J = 8 Hz, aromatic), 7.03 (t, 1H, J = 8 Hz, aromatic), 7.36 (dt, 1H, J_1 = 8 Hz, J_2 = 2 Hz, aromatic), 7.86 (br s, 1H), 8.15 (dd, 1H, J_1 = 8 Hz, J_2 = 1.5 Hz, aromatic). HRMS-ESI for C$_{24}$H$_{33}$NO$_2$ (*m/z*): [M+Na]$^+$ calcd, 390.2404; found, 390.2399; [2M+Na]$^+$ calcd, 757.4915; found, 757.4922.

N-(Adamantan-1-yl)-4-methoxybenzamide (**28**). Iodomethane (0.442 mmol, 0.063 g) was used for the methylation of compound **18**. The title compound was obtained as a white solid with a 42 % yield; mp, 152-154 °C. ^{1}H-NMR (300 MHz, CDCl$_3$) δ: 1.68-1.74 (m, 6H), 2.11-2.13 (m, 9H), 3.83 (s, 3H), 5.73 (br s, 1H), 6.89 (d, 2H, J = 6 Hz, aromatic), 7.67 (d, 2H, J = 6 Hz, aromatic). HRMS-ESI for C$_{18}$H$_{23}$NO$_2$ (*m/z*): [M+Na]$^+$ calcd, 308.1621; found, 308.1624; [2M+Na]$^+$ calcd, 593.3350; found, 593.3356.

N-(Adamantan-1-yl)-2,3-dimethoxybenzamide (**29**). Iodomethane (0.797 mmol, 0.113 g) was used for the methylation of compound **19**. The title compound was obtained as a white solid with a 60 % yield; mp, 140-142 °C. ^{1}H-NMR (500 MHz, CDCl$_3$) δ: 1.68-1.72 (m, 6H), 2.11-2.13 (m, 9H), 3.85 (s, 3H),

3.86 (s, 3H), 6.97-7.00 (m, 1H, aromatic), 7.10-7.14 (m, 1H, aromatic), 7.62 (dd, 2H, J_1= 8.0 Hz, J_2=1.6 Hz, aromatic), 7.81 (br s, 1H). HRMS-ESI for $C_{19}H_{25}NO_3$ (*m/z*): $[M+Na]^+$ calcd, 338.1727; found, 338.1740; $[2M+Na]^+$ calcd, 653.3572; found, 653.3595.

Biology

Materials. Cell culture reagents were purchased from Celbio s.r.l. (Milano, Italy). CulturePlate 96/wells plates were purchased from PerkinElmer Life Science; GW405833 and (R)-(þ)-WIN 55,212-2 were obtained from TOCRIS (Milan, Italy); Multiscreen HTS filter plates were purchased by Merck Millipore (Ireland). OptiPhase Supermix and $[^3H]$-CP55940 were purchased from PerkinElmer Life Science. COSTAR flat black plates were purchased from Sigma Aldrich. FAAH human recombinant enzyme and its substrate 7-amino-4-methyl-2*H*-1-benzopyran-2-one-5Z,8Z,11Z,14Z-eicosatetraen-amide, AMC-AA were purchased from Cayman Chemical, Ann Arbor, MI, USA. Ferrozine and NKH 477 were obtained from Sigma-Aldrich-RBI s.r.l. (Milan, Italy). Clear 96-wells microplate was purchased from Greiner Bio-One Italia S.r.l. (Milan, Italy).

Cell cultures. CB2R-HEK293 and CB1R-HEK293 cells were grown in DMEM high glucose supplemented with 10% fetal bovine serum, 2 mM glutamine,100 U/mL penicillin,100 mg/mL streptomycin, 0.1 mg/mL G418, in a humidified incubator at 37 °C with a 5% CO2 atmosphere. Human monocyte THP-1 cells were obtained from ATCC (Manassas, VA) and seeded at 1 x 10^5 cells/ml for 48 h. To differentiate cells into macrophages, 0.01 µM PMA was added for 48 h. By microscope analysis, in these conditions > 98% cells became adherent. To stimulate THP-1 monocytes and adherent cells, 10 µg/ml of LPS was added for 24 h, according to the protocol of differentitaion and actibation reported in Dreskin *et al.*[62] Cells were cultured in RPMI-1640 medium supplemented with 10% fetal bovine serum, 2 mM glutamine,100 U/mL penicillin,100 mg/mL streptomycin, in a humidified incubator at 37 °C with a 5% CO2 atmosphere.[62]

Radioligand binding assay

Membrane preparations for CB1 and CB2 receptors assays. Membranes of HEK293 cells recombinantly expressing the human CB1 receptor subtype, were prepared by scratching the cells off the previously frozen cell culture dishes in Phosphate Buffered Saline (PBS, pH 7.4). The cell suspension was centrifuged at 800xg for 15 min and the pellet was resuspended and homogenized on ice for 1 min using a dounce homogenizer, and subsequently spun down for 5 min at 4 °C and 500 g. The supernatant was centrifuged for 20 min at 25,000 g. The obtained membrane pellets were resuspended in buffer A (NaHCO$_3$10 mM, EGTA 10 mM, EDTA 10 mM, protease inhibitors cocktail 1X (Sigma Aldrich), pH 7.4) and centrifuged for 20 min at 25,000 g. The pellet was resuspended in the required amount of Tris-HCl buffer25 mM, MgCl$_2$ 5 mM, EDTA 1mM, pH 7.4. Aliquots of the membrane preparation were stored at -80°C until being used.[63] Membranes of HEK293 cells recombinantly expressing the human CB2 receptor subtypes were prepared by scratching the cells off the previously frozen cell culture dishes in ice-cold hypotonic buffer (Tris-HCl5 mM, EDTA, 2 mM, pH 7.4). The cell suspension was homogenized on ice for 1 min using an Ultra-Turrax (T25basic, IKALABORTECHNIK, Higashiosaka, Japan) followed by further homogenization for 1 min with a dounce homogenizer, and subsequently spun down for 10 min at 4 °C and 1000 g. The supernatant was centrifuged for 60 min at 48,000 g. The obtained membrane pellets were resuspended and homogenized in the required amount of Tris-HCl 50 mM buffer, pH 7.4. Aliquots of the membrane preparation were stored at -80 °C until being used.[63]

Radioligand competition binding assays at CB2 and CB1 receptors. Competition binding assays were performed as reported in Spinelli *et al.*[63] The membrane preparations of the HEK293 cells stably

expressing CB receptor subtype 2 (50 μg protein/well) was used as source for human CB2 receptor and as radioligand the CB agonist [³H](-)-*cis*-3-[2-hydroxy-4-(1,1-dimethylheptyl)phenyl]-*trans*-4-(3-hydroxypropyl)cyclohexanol (CP55,940), PerkinElmer Italia SPA, Milano, Italy). After addition of 25 μL of the test compounds at different concentrations (10^{-12}-10^{-5}M), 25 μL of [³H]-CP55,940 solution in assay buffer (at final concentration of 0.2 nM), and 100 μL of membrane preparation to 100 μL of assay buffer (Tris-HCl 50 mM, EGTA 2.5mM, MgCl₂ 5mM, fatty acid fere bovine serum albumine BSA 0.1%, pH 7.4), the suspension was incubated for 90 min at 30 °C. Total binding was determined without the test compounds. Nonspecific binding was determined in the presence of 10 μM GW405833, CB2R reference compound. The incubation was stopped by rapid filtration through a GF/C glass fibre filter (Merck Millipore, Ireland) presoaked for 30 min with 0.05% aq. Polyethyleneimine solution, using a 96-channel cell harvester (Merck Millipore, Ireland). The filter was washed three times with 100 μL ice-cold washing buffer (Tris-HCl 50 mM, EGTA 2.5 mM, MgCl₂ 5 mM, BSA 1%, pH 7.4), and then dried for 1.5 h at 50 °C. Radioactivity on the filter was determined in a MicroBeta JET counter (Perkin- Elmer, Boston, MA, USA) after 6 h of preincubation with 100 μl of scintillation cocktail (OptiPhase superMix, Perkin- Elmer). Data were obtained in three independent experiments, performed in triplicates. Data were analyzed using GraphPad Prism Version 7 (San Diego, CA, USA). For the calculation of K_i values, the Cheng-Prusoff equation and a K_d value of 1.5 nM ([³H]-CP55,940 at CB2) were used. Cannabinoid CB1 receptor competition binding experiments were carried out in a polypropylene 96-well plate. In each well 20 μg of membranes from HEK 293-hCB1 cell line, 0.8 nM [³H]-CP55940 (164.9 Ci/mmol, 1 mCi/mL, Perkin Elmer NET1051250UC) and studied and standard compounds were incubated. Non-specific binding was determined in the presence of Surinabant 10 μM. The reaction mixture was incubated at 30 °C for 60 min, 200 μL were transferred to GF/C 96-well plate (Millipore, Madrid, Spain) pretreated with binding buffer (Tris-HCl 50 mM, EDTA 1 mM, MgCl₂ 5 mM, BSA 0.5%, pH 7.4), afterwards it was filtered and washed four times with 250 μL wash buffer (Tris-HCl 50 mM, EDTA 1 mM, MgCl₂ 5 mM, BSA 0.5%, pH 7.4), before measuring in a microplate beta scintillation counter (Microbeta Trilux, PerkinElmer, Madrid, Spain). Data were obtained in three independent experiments, performed in triplicates.

Functional Activity at CB2R In Vitro. Gi-coupled cAMP modulation was measured following the manufacturer's protocol (Eurofins, Fremont, CA) as previously reported.[64] Briefly, CHO-K1 cells overexpressing the human CB2R were plated into a 96-well plate (30 000 cells/well) and incubated overnight at 37 °C, 5% CO2. Media was aspirated and replaced with 30 μL of assay buffer. Cells were incubated for 30 min at 37 °C with 15 μL of 3× dose−response solutions of samples prepared in the presence of a cell assay buffer containing 3× of 25 μM NKH-477 solution to stimulate adenylate cyclase and enhance basal cAMP levels. For all protocols, following stimulation, cell lysis and cAMP detection were performed as per the manufacturer's protocol. Luminescence measurements were performed using a GloMax Multi Detection System (Promega, Italy). Data are reported as means ± SEM of three independent experiments conducted in triplicate and were normalized considering the NKH-477 stimulus alone as 100% of the response. Data were analyzed using PRISM.9.3 software (GraphPad Software Inc, San Diego, CA).

FAAH enzyme inhibition assay. Assays were performed using 96-well black flat-bottom microtiter NBS plates (COSTAR flat black). The experiments were conducted in a total volume of 200 μl, first incubating different concentrations of each potential inhibitor in an appropriate fluorometric assay buffer (Tris-HCl 125 mM, Na₂EDTA 2H₂O 1 mM, pH=9.0) with the enzyme (FAAH Human recombinant, Cayman Chemical, Ann Arbor, MI, USA) for 10 min at room temperature, keeping the plate in orbital shaking. The substrate (7-amino-4-methyl-2*H*-1-benzopyran-2-one-5Z,8Z,11Z,14Z-

eicosatetraen-amide, AMC-AA, 1 µM final concentration) was then added, and the assay was incubated for 2 hours at 37 °C in a TECAN infinite M1000Pro plate reader (Tecan, Männedorf, Switzerland) which measured the fluorescence from each well every 30 seconds (λex = 340 nm, λem = 450 nm), determining FAAH activity as relative fluorescence units (RFU). Control wells lacking the inhibitor and blank wells lacking both inhibitor and enzyme were used to calculate percent inhibition for each tested compound. IC_{50} values were calculated via GraphPad Prism 5.0 (GraphPad Software, La Jolla, CA, USA) and are reported as mean ± SEM of at least three independent measurements performed in triplicate.

Measurement of activation status of the target GPCR by detecting β-arrestin. CB2- mediated β-arrestin recruitment experiments were carried out in mouse CB2 receptor transfected in CHO-K1 cell line provided in the PathHunter eXpress mCNR2 CHO-K1 β-Arrestin GPCR Assay kit (Discover X (93-047E2)[65]). 48 hours before the assay, cells were seeded on a 96 well white plate (supplied by kit) using the medium provided. Test compounds were added in AssayComplete Cell Plating Reagent and incubated for 90 minutes at 37 °C and 5% CO_2. After incubation, Working Detection Solution was added to each well and the plate was incubated for 60 minutes at RT. After this time, luminiscence due to β-arrestin recruitment (1000 ms) was measured in Perkin Elmer EnSpire Multimode plate reader. Data was normalized to the maximum effect observed with CP55940 and fitted to a 4-parameter logistic equation by employing GraphPad Prism.

Anti-inflammatory and pro-inflammatory cytochine detection. The amount of cytokines was measured in 5 µL of supernatants, derived from 1×10^4 cells, using the ProQuantum immunoassays kits for TNF-α, IFN-γ, IL-1β, IL-6, IL-10, IL-4, IL-17A (all from ThermoFisher Scientific (Waltham, MA), according to the manufacturer's instructions. The results were expressed as pg/ml based on the titration curved of each kits.

Functional Activity at CB1R in vitro. Human Cannabinoide CB1 receptor functional experiments were carried out in CHO-CB1 C3 cell line. 8000 cells were seeded in 100µl culture medium with dialyzed FBS (Sigma F0392) on a 96 well white plate half area (Costar 3688). Cells were preincubated for 15 minutes at 37°C. Test compounds and CP55.940 (control) were added in their corresponding wells and incubated for 15 minutes at 37 °C. Then, Forskolin 10µM (Sigma 17018) was added and incubated for 5 minutes at 37 °C. Reagents from the kit (#CISBIO 62AM4PEC) were added and after incubation for 1 hour at RT with gentle stirring (90 rpm) and protected from light, HTRF (λ_{Ex}: 320nm; λ_{Em}: 620-665nm) from each well was measured using a Tecan Infinite M1000 Pro.

Ferrozine-based assay. Determination of Fe^{2+}-chelation properties of novel CB2R compouds was performed using the iron chelation assay as reported in Pati et al. 2015 with minor modifications.[50] In this assay the ferrozine probe is used for its ability to chelate iron(II) species forming a colorimetric complex. Compounds able to chelate iron(II) subtract the ion from the ferrozine reducing the complex formation and thus the colorimetric measure. Ferrozine probe reacts with divalent iron to form stable magenta species. The maximum absorbance is recorded at a wavelength of 562 nm. Into clear 96-wells plate, 25 µM of $FeSO_4$ dissolved in water was incubated with or without tested compound (100 µM, in DMSO) for 15 min at room temperature in a final volume of 300 µL. After the established incubation time, ferrozine dissolved in water (1 mM final concentration) was added. The plate was shaken for 15 min at room temperature. The absorbance values at 562 was determined on the microplate reader Victor 3 from PerkinElmer Life Sciences.

Statistical analysis. All data in the text and figures are provided as means ± SEM. The results were analysed ANOVA test, using Graph-Pad Prism (Graph-Pad software, San Diego, CA, USA). $p < 0.05$ was considered significant.

Molecular docking simulations. **13**, **14, 15, 25, 26** and **27** were docked on the recently published X-ray structures of CB2R in complex with the agonist AM12033 (resolution 3.20 Å - PDB code: 6KPC[52]). Furthermore **13, 26** and **27** were also docked on the X-ray structure of humanized rat FAAH in complex with the non-covalent inhibitor **JXV** (Resolution 2.77 Å - PDB code: 6MRG[57]) and the X-ray structure showing the CB1R receptor complexed with the agonist AM11542 (PDB code: 5XRA[55]). The retrieved files were prepared using the Protein Preparation Wizard tool,[66] available from the Schrodinger Suite 2021-2, to add missing hydrogen atoms, reconstruct incomplete side chains, assign favourable protonation states at physiological pH, remove water molecules, optimize the hydrogen bonding network and performing a force field-based minimization (OPLS-4[67]) of the 3D protein structures. All the ligands were subjected to LigPrep,[68] a tool available from the Schrodinger Suite 2021-2, to desalt and generate all the tautomers and ionization states at a pH value of 7.0 ± 2.0. The obtained files were employed for standard docking simulations performed by Grid-based ligand docking with energetics[69] (GLIDE), holding the protein fixed, but allowing full flexibility for the ligands. In all cases, a cubic grid was generated on the centroid of the cognate ligand. In doing that, we obtained an inner box of 10 Å × 10 Å × 10 Å irrespective of the considered protein structure and an outer box of 26 Å × 26 Å × 26 Å, 24 Å × 24 Å × 24 Å, and 28 Å × 28 Å × 28 Å in 6KPC, 5XRA and 6MRG respectively. All docking simulations were performed using the default force field OPLS_2005[70] and the extra precision docking (XP) protocol. In addition, for docking simulations performed on 6DK1 (CB2R) and 5XRA (CB1R), we used an expanded sampling; for computations performed on 6MRG (FAAH), the number of generated poses per ligand in the initial phase of docking was increased from 5000 (default setting) to 50000 along with the number of those kept for energy minimization from 800 (default setting) to 8000, to properly explore the conformational space of the ligands during the simulations. Importantly, such protocols were validated by redocking the cognate ligands (RMSD = 0.71 Å for AM12033, RMSD = 0.50 Å for AM11542, and RMSD = 1.25 Å for JXV).

MM-GBSA calculations. All the obtained complexes from performed simulations were subjected to molecular mechanics/generalized Born surface area calculations (MM-GBSA[71]), following an approach recently published.[72] This protocol allows computing the binding free energies (ΔG) of the protein-ligand complexes. During this calculation, flexibility was allowed for all residues having at least one atom within a distance of 5 Å from the ligand

AUTHOR INFORMATION

Corresponding Authors:

Marialessandra Contino − *Dipartimento di Farmacia-Scienze del Farmaco, Università degli Studi di Bari ALDO MORO, via Orabona 4, 70125, Bari, Italy*; https://orcid.org/0000-0002-0713-3151; Phone: +39-080 5442751; Email: marialessandra.contino@uniba.it

Carmen Abate - *Dipartimento di Farmacia-Scienze del Farmaco, Università degli Studi di Bari ALDO MORO, via Orabona 4, 70125, Bari, Italy*; *[b]Institute of Crystallography, National Research Council of Italy, Via Amendola, 122/o, 70126 Bari;* https://orcid.org/0000-0001-9292-884X; Phone: +39-080-5442727; Email:carmen.abate@uniba.it

Authors

Francesca Intranuovo-*Dipartimento di Farmacia-Scienze del Farmaco, Università degli Studi di Bari ALDO MORO, via Orabona 4, 70125, Bari, Italy*

Leonardo Brunetti- *Dipartimento di Farmacia-Scienze del Farmaco, Università degli Studi di Bari ALDO MORO, via Orabona 4, 70125, Bari, Italy*

Pietro DelRe-[b]*Institute of Crystallography, National Research Council of Italy, Via Amendola, 122/o, 70126 Bari, Italy*

Giuseppe Felice Mangiatordi-[b]*Institute of Crystallography, National Research Council of Italy, Via Amendola, 122/o, 70126 Bari, Italy*

Angela Stefanachi- *Dipartimento di Farmacia-Scienze del Farmaco, Università degli Studi di Bari ALDO MORO, via Orabona 4, 70125, Bari, Italy*

Antonio Laghezza- *Dipartimento di Farmacia-Scienze del Farmaco, Università degli Studi di Bari ALDO MORO, via Orabona 4, 70125, Bari, Italy*

Mauro Niso- *Dipartimento di Farmacia-Scienze del Farmaco, Università degli Studi di Bari ALDO MORO, via Orabona 4, 70125, Bari, Italy*

Francesco Leonetti- *Dipartimento di Farmacia-Scienze del Farmaco, Università degli Studi di Bari ALDO MORO, via Orabona 4, 70125, Bari, Italy*

Fulvio Loiodice- *Dipartimento di Farmacia-Scienze del Farmaco, Università degli Studi di Bari ALDO MORO, via Orabona 4, 70125, Bari, Italy*

Alessia Ligresti- *Institute of Biomolecular Chemistry, National Research Council of Italy, Via Campi Flegrei 34, 80078, Pozzuoli (Na), Italy*

Magdalena Kostrzewa-[c]*Institute of Biomolecular Chemistry, National Research Council of Italy, Via Campi Flegrei 34, 80078, Pozzuoli (Na), Italy*

Jose Brea-*Innopharma Screening Platform, BioFarma Research Group, Center for Research in Molecular Medicine and Chronic Diseases (CIMUS), University of Santiago de Compostela, Santiago de Compostela, Spain;[e] Department of Pharmacology, Pharmacy and Pharmaceutical Technology. School of Pharmacy. University of Santiago de Compostela, 1578, Santiago de Compostela, Spain*

Maria Isabel Loza- *Innopharma Screening Platform, BioFarma Research Group, Center for Research in Molecular Medicine and Chronic Diseases (CIMUS), University of Santiago de Compostela, Santiago de Compostela, Spain;[e] Department of Pharmacology, Pharmacy and Pharmaceutical Technology. School of Pharmacy. University of Santiago de Compostela, 15782, Santiago de Compostela, Spain*

Eddy Sotelo Perez- *ComBioMed Research Group, Centro de Química Biológica y Materiales Moleculares (CIQUS) University of Santiago de Compostela, Santiago de Compostela, Spain;*

Michele Saviano- *Institute of Crystallography, National Research Council of Italy, Via Vivaldi, 43, 81100, Caserta, Italy*

Nicola Antonio Colabufo- *Dipartimento di Farmacia-Scienze del Farmaco, Università degli Studi di Bari ALDO MORO, via Orabona 4, 70125, Bari, Italy*

Chiara Riganti-*Dipartimento di Oncologia, Università degli Studi di Torino, 10126, Torino, Italy*

ABBREVIATIONS

AD, Alzheimer's disease; ANOVA, analysis of variance; BSA, bovine serum albumin; cAMP, cyclic adenosine monophosphate; CB2R, cannabinoid receptor subtype 2; CB1R, cannabinoid receptor subtype 1; $CDCl_3$, deuterated chloroform; CNS, Central Nervous, System; DIPEA, N,N-diisopropylethylamine; DMF, dimethylformamide; DMSO-d6 , deuterated dimethyl sulfoxide; EC_{50}, maximal effective concentration; ECS, Endocannabinoid system; EDTA, ethylenediaminetetraacetic acid; ELISA, enzyme-linked immunosorbent assay; FAAH, Fatty Acid Amide Hydrolase; HBTU, N,N,N′,N′-tetramethyl-O-(1H-benzotriazol-1-yl)uronium hexafluorophosphate; HBTU, 3-[Bis(dimethylamino)methyliumyl]-3H-benzotriazol-1-oxide hexafluorophosphate; Hz, hertz; HPLC, high performance liquid chromatography; IFN-γ, Interferon Gamma; IL-1β, Interleukin 1 beta; IL-4, Interleukin 4; IL-6, Interleukin 6; IL-10, Interleukin 10; *J*, coupling constant; *K*i, inhibitor constant; LPS, lipopolysaccharide; MHz, megahertz; MMGBSA, generalized Born and surface area continuum solvation method;MMGBSA lipo, lipophilic binding energy; MMGBSA vdw, Van der Waals binding energy; mmol, millimole; μL, microliter; μM, micromolar; nM, nanomolar; NKH-477, Colforsin daropate hydrochloride; NMR, nuclear magnetic resonance; PCA, Principal Component Analysis; PBS, phosphate buffered saline; DMEM, Dulbecco's modified eagle medium; PDB, code protein data bank; PMA, phorbol 12-myristate 13-acetate; Ppm, parts per million; PPW, protein preparation wizard; qRT-PCR, real-time polymerase chain reaction; Rt, room temperature; SEM, standard error of mean; TNFα, Tumor necrosis factor alpha; THP-1, human monocytic cell line derived from an acute monocytic leukemia patient.

ASSOCIATED CONTENT

SUPPORTING INFORMATION

Molecular Formula String; Pharmacokinetic profile of compounds **13**, **26**, and **27** according to BoiledEgg; P-glycoprotein interaction assay; Ferrozine assay for all final compounds; Top-scored docking poses returned by docking simulations performed on **13**, **26**, **27** within the binding site of CB1R; List of the Computed MMGBSA scores from docking simulations at CB2R, CB1R, and FAAH; HPLC traces for representative final compounds; 1HNMR spectra for representative final compounds.

References

(1) Di Marzo, V. The Endocannabinoidome as a Substrate for Noneuphoric Phytocannabinoid Action and Gut Microbiome Dysfunction in Neuropsychiatric Disorders. *Dialogues Clin Neurosci* **2020**, *22* (3), 259–269. https://doi.org/10.31887/DCNS.2020.22.3/vdimarzo.

(2) Di Marzo, V.; Piscitelli, F. The Endocannabinoid System and Its Modulation by Phytocannabinoids. *Neurotherapeutics* **2015**, *12* (4), 692–698. https://doi.org/10.1007/s13311-015-0374-6.

(3) Contino, M.; McCormick, P. J. Editorial: The Canonical and Non-Canonical Endocannabinoid System as a Target in Cancer and Acute and Chronic Pain. *Front Pharmacol* **2020**, *11*, 312. https://doi.org/10.3389/fphar.2020.00312.

(4) Cristino, L.; Bisogno, T.; Di Marzo, V. Cannabinoids and the Expanded Endocannabinoid System in Neurological Disorders. *Nat Rev Neurol* **2020**, *16* (1), 9–29. https://doi.org/10.1038/s41582-019-0284-z.

(5) Spinelli, F.; Capparelli, E.; Abate, C.; Colabufo, N. A.; Contino, M. Perspectives of Cannabinoid Type 2 Receptor (CB2R) Ligands in Neurodegenerative Disorders: Structure–Affinity Relationship (SAfiR) and Structure–Activity Relationship (SAR) Studies. *J. Med. Chem.* **2017**, *60* (24), 9913–9931. https://doi.org/10.1021/acs.jmedchem.7b00155.

(6) Zhang, J.; Zhang, S.; Liu, Y.; Su, M.; Ling, X.; Liu, F.; Ge, Y.; Bai, M. Combined CB2 Receptor Agonist and Photodynamic Therapy Synergistically Inhibit Tumor Growth in Triple Negative Breast Cancer. *Photodiagnosis Photodyn Ther* **2018**, *24*, 185–191. https://doi.org/10.1016/j.pdpdt.2018.09.006.

(7) Kisková, T.; Mungenast, F.; Suváková, M.; Jäger, W.; Thalhammer, T. Future Aspects for Cannabinoids in Breast Cancer Therapy. *Int J Mol Sci* **2019**, *20* (7), 1673. https://doi.org/10.3390/ijms20071673.

(8) Morales, P.; Jagerovic, N. Antitumor Cannabinoid Chemotypes: Structural Insights. *Front Pharmacol* **2019**, *10*, 621. https://doi.org/10.3389/fphar.2019.00621.

(9) Rastegar, M.; Samadizadeh, S.; Yasaghi, M.; Moradi, A.; Tabarraei, A.; Salimi, V.; Tahamtan, A. Functional Variation (Q63R) in the Cannabinoid CB2 Receptor May Affect the Severity of COVID-19: A Human Study and Molecular Docking. *Arch Virol* **2021**, *166* (11), 3117–3126. https://doi.org/10.1007/s00705-021-05223-7.

(10) Rb, van B.; Rn, M.; Ta, B.; Jb, W.; Hc, L.; S, F.; Fg, T. Cannabinoids Block Cellular Entry of SARS-CoV-2 and the Emerging Variants. *Journal of natural products* **2022**, *85* (1). https://doi.org/10.1021/acs.jnatprod.1c00946.

(11) Nagoor Meeran, M. F.; Sharma, C.; Goyal, S. N.; Kumar, S.; Ojha, S. CB2 Receptor-selective Agonists as Candidates for Targeting Infection, Inflammation, and Immunity in SARS-CoV-2 Infections. *Drug Dev Res* **2020**, 10.1002/ddr.21752. https://doi.org/10.1002/ddr.21752.

(12) Jha, N. K.; Sharma, C.; Hashiesh, H. M.; Arunachalam, S.; Meeran, M. N.; Javed, H.; Patil, C. R.; Goyal, S. N.; Ojha, S. β-Caryophyllene, A Natural Dietary CB2 Receptor Selective Cannabinoid Can Be a Candidate to Target the Trinity of Infection, Immunity, and Inflammation in COVID-19. *Front Pharmacol* **2021**, *12*, 590201. https://doi.org/10.3389/fphar.2021.590201.

(13) Rossi, F.; Tortora, C.; Argenziano, M.; Di Paola, A.; Punzo, F. Cannabinoid Receptor Type 2: A Possible Target in SARS-CoV-2 (CoV-19) Infection? *Int J Mol Sci* **2020**, *21* (11), 3809. https://doi.org/10.3390/ijms21113809.

(14) Mangiatordi, G. F.; Intranuovo, F.; Delre, P.; Abatematteo, F. S.; Abate, C.; Niso, M.; Creanza, T. M.; Ancona, N.; Stefanachi, A.; Contino, M. Cannabinoid Receptor Subtype 2 (CB2R) in a Multitarget Approach: Perspective of an Innovative Strategy in Cancer and Neurodegeneration. *J Med Chem* **2020**, *63* (23), 14448–14469. https://doi.org/10.1021/acs.jmedchem.0c01357.

(15) Creanza, T. M.; Lamanna, G.; Delre, P.; Contino, M.; Corriero, N.; Saviano, M.; Mangiatordi, G. F.; Ancona, N. DeLA-Drug: A Deep Learning Algorithm for Automated Design of Druglike Analogues. *J. Chem. Inf. Model.* **2022**. https://doi.org/10.1021/acs.jcim.2c00205.

(16) Ashton, J. C.; Glass, M. The Cannabinoid CB2 Receptor as a Target for Inflammation-Dependent Neurodegeneration. *Curr Neuropharmacol* **2007**, *5* (2), 73–80.

(17) Benito, C.; Núñez, E.; Tolón, R. M.; Carrier, E. J.; Rábano, A.; Hillard, C. J.; Romero, J. Cannabinoid CB2 Receptors and Fatty Acid Amide Hydrolase Are Selectively Overexpressed in Neuritic Plaque-

Associated Glia in Alzheimer's Disease Brains. *J Neurosci* **2003**, *23* (35), 11136–11141. https://doi.org/10.1523/JNEUROSCI.23-35-11136.2003.

(18) Jain, S.; Bisht, A.; Verma, K.; Negi, S.; Paliwal, S.; Sharma, S. The Role of Fatty Acid Amide Hydrolase Enzyme Inhibitors in Alzheimer's Disease. *Cell Biochem Funct* **2022**, *40* (2), 106–117. https://doi.org/10.1002/cbf.3680.

(19) Petrosino, S.; Schiano Moriello, A. Palmitoylethanolamide: A Nutritional Approach to Keep Neuroinflammation within Physiological Boundaries-A Systematic Review. *Int J Mol Sci* **2020**, *21* (24), E9526. https://doi.org/10.3390/ijms21249526.

(20) van Esbroeck, A. C. M.; Janssen, A. P. A.; Cognetta, A. B.; Ogasawara, D.; Shpak, G.; van der Kroeg, M.; Kantae, V.; Baggelaar, M. P.; de Vrij, F. M. S.; Deng, H.; Allarà, M.; Fezza, F.; Lin, Z.; van der Wel, T.; Soethoudt, M.; Mock, E. D.; den Dulk, H.; Baak, I. L.; Florea, B. I.; Hendriks, G.; De Petrocellis, L.; Overkleeft, H. S.; Hankemeier, T.; De Zeeuw, C. I.; Di Marzo, V.; Maccarrone, M.; Cravatt, B. F.; Kushner, S. A.; van der Stelt, M. Activity-Based Protein Profiling Reveals off-Target Proteins of the FAAH Inhibitor BIA 10-2474. *Science* **2017**, *356* (6342), 1084–1087. https://doi.org/10.1126/science.aaf7497.

(21) Gado, F.; Arena, C.; Fauci, C. L.; Reynoso-Moreno, I.; Bertini, S.; Digiacomo, M.; Meini, S.; Poli, G.; Macchia, M.; Tuccinardi, T.; Gertsch, J.; Chicca, A.; Manera, C. Modification on the 1,2-Dihydro-2-Oxo-Pyridine-3-Carboxamide Core to Obtain Multi-Target Modulators of Endocannabinoid System. *Bioorganic Chemistry* **2020**, *94*, 103353. https://doi.org/10.1016/j.bioorg.2019.103353.

(22) Pietrangolini, G.; Donzelli, F.; Berlanda, D.; Allegrini, Pietro; Rossignoli, Andrea; Stucchi, Michela; Riva, Antonella. Targeting Cannabinoid Receptors and Fatty Acid Amide Hydrolase: An Innovative Food-Grade Delivery System of Zingiber Officinale and Acmella Oleracea Extracts as Natural Adjuvant in Pain Management. *Targeting Cannabinoid Receptors and Fatty Acid Amide Hydrolase: An Innovative Food-Grade Delivery System of Zingiber officinale and Acmella oleracea Extracts as Natural Adjuvant in Pain Management*. p Volume 10, Issue 1.

(23) Davies, M.; Nowotka, M.; Papadatos, G.; Dedman, N.; Gaulton, A.; Atkinson, F.; Bellis, L.; Overington, J. P. ChEMBL Web Services: Streamlining Access to Drug Discovery Data and Utilities. *Nucleic Acids Research* **2015**, *43* (W1), W612–W620. https://doi.org/10.1093/nar/gkv352.

(24) Lucchesi, V.; Parkkari, T.; Savinainen, J. R.; Malfitano, A. M.; Allarà, M.; Bertini, S.; Castelli, F.; Del Carlo, S.; Laezza, C.; Ligresti, A.; Saccomanni, G.; Bifulco, M.; Di Marzo, V.; Macchia, M.; Manera, C. 1,2-Dihydro-2-Oxopyridine-3-Carboxamides: The C-5 Substituent Is Responsible for Functionality Switch at CB2 Cannabinoid Receptor. *Eur J Med Chem* **2014**, *74*, 524–532. https://doi.org/10.1016/j.ejmech.2013.10.070.

(25) Lachowicz, J. I.; Crespo-Alonso, M.; Caltagirone, C.; Alberti, G.; Biesuz, R.; Orton, J. O.; Nurchi, V. M. Salicylamide Derivatives for Iron and Aluminium Sequestration. From Synthesis to Complexation Studies. *Journal of Trace Elements in Medicine and Biology* **2018**, *50*, 580–588. https://doi.org/10.1016/j.jtemb.2018.04.010.

(26) Sheng, R.; Tang, L.; Jiang, L.; Hong, L.; Shi, Y.; Zhou, N.; Hu, Y. Novel 1-Phenyl-3-Hydroxy-4-Pyridinone Derivatives as Multifunctional Agents for the Therapy of Alzheimer's Disease. *ACS Chem. Neurosci.* **2016**, *7* (1), 69–81. https://doi.org/10.1021/acschemneuro.5b00224.

(27) Bakhoda, A. (Gus); Jiang, Q.; Badiei, Y. M.; Bertke, J. A.; Cundari, T. R.; Warren, T. H. Copper-Catalyzed C(Sp3)−H Amidation: Sterically Driven Primary and Secondary C−H Site-Selectivity. *Angewandte Chemie International Edition* **2019**, *58* (11), 3421–3425. https://doi.org/10.1002/anie.201810556.

(28) Moon, Y.; Jeong, Y.; Kook, D.; Hong, S. Rh(III)-Catalyzed Direct C−H/C−H Cross-Coupling of Quinones with Arenes Assisted by a Directing Group: Identification of Carbazole Quinones as GSKβ Inhibitors. *Org. Biomol. Chem.* **2015**, *13* (13), 3918–3923. https://doi.org/10.1039/C4OB02624A.

(29) Pasquini, S.; Botta, L.; Semeraro, T.; Mugnaini, C.; Ligresti, A.; Palazzo, E.; Maione, S.; Di Marzo, V.; Corelli, F. Investigations on the 4-Quinolone-3-Carboxylic Acid Motif. 2. Synthesis and Structure−Activity Relationship of Potent and Selective Cannabinoid-2 Receptor Agonists Endowed with Analgesic Activity in Vivo. *J. Med. Chem.* **2008**, *51* (16), 5075–5084. https://doi.org/10.1021/jm800552f.

(30) Baramov, T.; Schmid, B.; Ryu, H.; Jeong, J.; Keijzer, K.; von Eckardstein, L.; Baik, M.-H.; Süssmuth, R. D. How Many O-Donor Groups in Enterobactin Does It Take to Bind a Metal Cation? *Chemistry – A European Journal* **2019**, *25* (28), 6955–6962. https://doi.org/10.1002/chem.201900453.

(31) Kühl, N.; Leuthold, M. M.; Behnam, M. A. M.; Klein, C. D. Beyond Basicity: Discovery of Nonbasic DENV-2 Protease Inhibitors with Potent Activity in Cell Culture. *J. Med. Chem.* **2021**, *64* (8), 4567–4587. https://doi.org/10.1021/acs.jmedchem.0c02042.

(32) Abergel, R. J.; Warner, J. A.; Shuh, D. K.; Raymond, K. N. Enterobactin Protonation and Iron Release: Structural Characterization of the Salicylate Coordination Shift in Ferric Enterobactin1. *J. Am. Chem. Soc.* **2006**, *128* (27), 8920–8931. https://doi.org/10.1021/ja062046j.

(33) El-Gamal, M. I.; Zaraei, S.-O.; Foster, P. A.; Anbar, H. S.; El-Gamal, R.; El-Awady, R.; Potter, B. V. L. A New Series of Aryl Sulfamate Derivatives: Design, Synthesis, and Biological Evaluation. *Bioorganic & Medicinal Chemistry* **2020**, *28* (8), 115406. https://doi.org/10.1016/j.bmc.2020.115406.

(34) Kenakin, T. Biased Receptor Signaling in Drug Discovery. *Pharmacol Rev* **2019**, *71* (2), 267–315. https://doi.org/10.1124/pr.118.016790.

(35) Shchepinova, M. M.; Hanyaloglu, A. C.; Frost, G. S.; Tate, E. W. Chemical Biology of Noncanonical G Protein-Coupled Receptor Signaling: Toward Advanced Therapeutics. *Curr Opin Chem Biol* **2020**, *56*, 98–110. https://doi.org/10.1016/j.cbpa.2020.04.012.

(36) Seyedabadi, M.; Ghahremani, M. H.; Albert, P. R. Biased Signaling of G Protein Coupled Receptors (GPCRs): Molecular Determinants of GPCR/Transducer Selectivity and Therapeutic Potential. *Pharmacol Ther* **2019**, *200*, 148–178. https://doi.org/10.1016/j.pharmthera.2019.05.006.

(37) Brogi, S.; Tafi, A.; Désaubry, L.; Nebigil, C. G. Discovery of GPCR Ligands for Probing Signal Transduction Pathways. *Frontiers in Pharmacology* **2014**, *5*.

(38) Correll, C. C.; McKittrick, B. A. Biased Ligand Modulation of Seven Transmembrane Receptors (7TMRs): Functional Implications for Drug Discovery. *J Med Chem* **2014**, *57* (16), 6887–6896. https://doi.org/10.1021/jm401677g.

(39) Tan, L.; Yan, W.; McCorvy, J. D.; Cheng, J. Biased Ligands of G Protein-Coupled Receptors (GPCRs): Structure–Functional Selectivity Relationships (SFSRs) and Therapeutic Potential. *J. Med. Chem.* **2018**, *61* (22), 9841–9878. https://doi.org/10.1021/acs.jmedchem.8b00435.

(40) Urban, J. D.; Clarke, W. P.; von Zastrow, M.; Nichols, D. E.; Kobilka, B.; Weinstein, H.; Javitch, J. A.; Roth, B. L.; Christopoulos, A.; Sexton, P. M.; Miller, K. J.; Spedding, M.; Mailman, R. B. Functional Selectivity and Classical Concepts of Quantitative Pharmacology. *J Pharmacol Exp Ther* **2007**, *320* (1), 1–13. https://doi.org/10.1124/jpet.106.104463.

(41) Shenoy, S. K.; Lefkowitz, R. J. β-Arrestin-Mediated Receptor Trafficking and Signal Transduction. *Trends Pharmacol Sci* **2011**, *32* (9), 521–533. https://doi.org/10.1016/j.tips.2011.05.002.

(42) Ibsen, M. S.; Finlay, D. B.; Patel, M.; Javitch, J. A.; Glass, M.; Grimsey, N. L. Cannabinoid CB1 and CB2 Receptor-Mediated Arrestin Translocation: Species, Subtype, and Agonist-Dependence. *Front Pharmacol* **2019**, *10*, 350. https://doi.org/10.3389/fphar.2019.00350.

(43) Cabral, G. A.; Dove Pettit, D. A. Drugs and Immunity: Cannabinoids and Their Role in Decreased Resistance to Infectious Disease. *J Neuroimmunol* **1998**, *83* (1–2), 116–123. https://doi.org/10.1016/s0165-5728(97)00227-0.

(44) Klein, T. W.; Newton, C.; Friedman, H. Cannabinoid Receptors and Immunity. *Immunology Today* **1998**, *19* (8), 373–381. https://doi.org/10.1016/S0167-5699(98)01300-0.

(45) Castaneda, J. T.; Harui, A.; Kiertscher, S. M.; Roth, J. D.; Roth, M. D. Differential Expression of Intracellular and Extracellular CB(2) Cannabinoid Receptor Protein by Human Peripheral Blood Leukocytes. *J Neuroimmune Pharmacol* **2013**, *8* (1), 323–332. https://doi.org/10.1007/s11481-012-9430-8.

(46) Chiurchiù, V.; Lanuti, M.; Catanzaro, G.; Fezza, F.; Rapino, C.; Maccarrone, M. Detailed Characterization of the Endocannabinoid System in Human Macrophages and Foam Cells, and Anti-Inflammatory Role of Type-2 Cannabinoid Receptor. *Atherosclerosis* **2014**, *233* (1), 55–63. https://doi.org/10.1016/j.atherosclerosis.2013.12.042.

(47) Du, Y.; Ren, P.; Wang, Q.; Jiang, S.-K.; Zhang, M.; Li, J.-Y.; Wang, L.-L.; Guan, D.-W. Cannabinoid 2 Receptor Attenuates Inflammation during Skin Wound Healing by Inhibiting M1 Macrophages Rather

than Activating M2 Macrophages. *J Inflamm (Lond)* **2018**, *15*, 25. https://doi.org/10.1186/s12950-018-0201-z.

(48) Manera, C.; Benetti, V.; Castelli, M. P.; Cavallini, T.; Lazzarotti, S.; Pibiri, F.; Saccomanni, G.; Tuccinardi, T.; Vannacci, A.; Martinelli, A.; Ferrarini, P. L. Design, Synthesis, and Biological Evaluation of New 1,8-Naphthyridin-4(1H)-on-3-Carboxamide and Quinolin-4(1H)-on-3-Carboxamide Derivatives as CB2 Selective Agonists. *J Med Chem* **2006**, *49* (20), 5947–5957. https://doi.org/10.1021/jm0603466.

(49) Long, J. Z.; Nomura, D. K.; Vann, R. E.; Walentiny, D. M.; Booker, L.; Jin, X.; Burston, J. J.; Sim-Selley, L. J.; Lichtman, A. H.; Wiley, J. L.; Cravatt, B. F. Dual Blockade of FAAH and MAGL Identifies Behavioral Processes Regulated by Endocannabinoid Crosstalk in Vivo. *Proc Natl Acad Sci U S A* **2009**, *106* (48), 20270–20275. https://doi.org/10.1073/pnas.0909411106.

(50) Pati, M. L.; Niso, M.; Ferorelli, S.; Abate, C.; Berardi, F. Novel Metal Chelators Thiosemicarbazones with Activity at the Σ2 Receptors and P-Glycoprotein: An Innovative Strategy for Resistant Tumor Treatment. *RSC Adv.* **2015**, *5* (125), 103131–103146. https://doi.org/10.1039/C5RA19857G.

(51) Huat, T. J.; Camats-Perna, J.; Newcombe, E. A.; Valmas, N.; Kitazawa, M.; Medeiros, R. Metal Toxicity Links to Alzheimer's Disease and Neuroinflammation. *J Mol Biol* **2019**, *431* (9), 1843–1868. https://doi.org/10.1016/j.jmb.2019.01.018.

(52) Hua, T.; Li, X.; Wu, L.; Iliopoulos-Tsoutsouvas, C.; Wang, Y.; Wu, M.; Shen, L.; Brust, C. A.; Nikas, S. P.; Song, F.; Song, X.; Yuan, S.; Sun, Q.; Wu, Y.; Jiang, S.; Grim, T. W.; Benchama, O.; Stahl, E. L.; Zvonok, N.; Zhao, S.; Bohn, L. M.; Makriyannis, A.; Liu, Z.-J. Activation and Signaling Mechanism Revealed by Cannabinoid Receptor-Gi Complex Structures. *Cell* **2020**, *180* (4), 655-665.e18. https://doi.org/10.1016/j.cell.2020.01.008.

(53) Deng, Z.; Chuaqui, C.; Singh, J. Structural Interaction Fingerprint (SIFt): A Novel Method for Analyzing Three-Dimensional Protein–Ligand Binding Interactions. *J. Med. Chem.* **2004**, *47* (2), 337–344. https://doi.org/10.1021/jm030331x.

(54) Creanza, T. M.; Delre, P.; Ancona, N.; Lentini, G.; Saviano, M.; Mangiatordi, G. F. Structure-Based Prediction of HERG-Related Cardiotoxicity: A Benchmark Study. *J. Chem. Inf. Model.* **2021**, *61* (9), 4758–4770. https://doi.org/10.1021/acs.jcim.1c00744.

(55) Hua, T.; Vemuri, K.; Nikas, S. P.; Laprairie, R. B.; Wu, Y.; Qu, L.; Pu, M.; Korde, A.; Jiang, S.; Ho, J.-H.; Han, G. W.; Ding, K.; Li, X.; Liu, H.; Hanson, M. A.; Zhao, S.; Bohn, L. M.; Makriyannis, A.; Stevens, R. C.; Liu, Z.-J. Crystal Structures of Agonist-Bound Human Cannabinoid Receptor CB1. *Nature* **2017**, *547* (7664), 468–471. https://doi.org/10.1038/nature23272.

(56) Mileni, M.; Johnson, D. S.; Wang, Z.; Everdeen, D. S.; Liimatta, M.; Pabst, B.; Bhattacharya, K.; Nugent, R. A.; Kamtekar, S.; Cravatt, B. F.; Ahn, K.; Stevens, R. C. Structure-Guided Inhibitor Design for Human FAAH by Interspecies Active Site Conversion. *Proceedings of the National Academy of Sciences* **2008**, *105* (35), 12820–12824. https://doi.org/10.1073/pnas.0806121105.

(57) Saha, A.; Shih, A. Y.; Mirzadegan, T.; Seierstad, M. Predicting the Binding of Fatty Acid Amide Hydrolase Inhibitors by Free Energy Perturbation. *J. Chem. Theory Comput.* **2018**, *14* (11), 5815–5822. https://doi.org/10.1021/acs.jctc.8b00672.

(58) Roughley, S. D. Five Years of the KNIME Vernalis Cheminformatics Community Contribution. *Current Medicinal Chemistry 27* (38), 6495–6522.

(59) O'Boyle, N. M.; Banck, M.; James, C. A.; Morley, C.; Vandermeersch, T.; Hutchison, G. R. Open Babel: An Open Chemical Toolbox. *Journal of Cheminformatics* **2011**, *3* (1), 33. https://doi.org/10.1186/1758-2946-3-33.

(60) Willighagen, E. L.; Mayfield, J. W.; Alvarsson, J.; Berg, A.; Carlsson, L.; Jeliazkova, N.; Kuhn, S.; Pluskal, T.; Rojas-Chertó, M.; Spjuth, O.; Torrance, G.; Evelo, C. T.; Guha, R.; Steinbeck, C. The Chemistry Development Kit (CDK) v2.0: Atom Typing, Depiction, Molecular Formulas, and Substructure Searching. *Journal of Cheminformatics* **2017**, *9* (1), 33. https://doi.org/10.1186/s13321-017-0220-4.

(61) Berthold, M. R.; Cebron, N.; Dill, F.; Gabriel, T. R.; Kötter, T.; Meinl, T.; Ohl, P.; Thiel, K.; Wiswedel, B. KNIME - the Konstanz Information Miner: Version 2.0 and Beyond. *SIGKDD Explor. Newsl.* **2009**, *11* (1), 26–31. https://doi.org/10.1145/1656274.1656280.

(62) Dreskin, S. C.; Thomas, G. W.; Dale, S. N.; Heasley, L. E. Isoforms of Jun Kinase Are Differentially Expressed and Activated in Human Monocyte/Macrophage (THP-1) Cells. *The Journal of Immunology* **2001**, *166* (9), 5646–5653. https://doi.org/10.4049/jimmunol.166.9.5646.

(63) Spinelli, F.; Giampietro, R.; Stefanachi, A.; Riganti, C.; Kopecka, J.; Abatematteo, F. S.; Leonetti, F.; Colabufo, N. A.; Mangiatordi, G. F.; Nicolotti, O.; Perrone, M. G.; Brea, J.; Loza, M. I.; Infantino, V.; Abate, C.; Contino, M. Design and Synthesis of Fluorescent Ligands for the Detection of Cannabinoid Type 2 Receptor (CB2R). *Eur J Med Chem* **2020**, *188*, 112037. https://doi.org/10.1016/j.ejmech.2020.112037.

(64) Mugnaini, C.; Kostrzewa, M.; Bryk, M.; Mahmoud, A. M.; Brizzi, A.; Lamponi, S.; Giorgi, G.; Ferlenghi, F.; Vacondio, F.; Maccioni, P.; Colombo, G.; Mor, M.; Starowicz, K.; Di Marzo, V.; Ligresti, A.; Corelli, F. Correction to Design, Synthesis, and Physicochemical and Pharmacological Profiling of 7-Hydroxy-5-Oxopyrazolo[4,3-b]Pyridine-6-Carboxamide Derivatives with Antiosteoarthritic Activity In Vivo. *J. Med. Chem.* **2020**, *63* (19), 11303–11303. https://doi.org/10.1021/acs.jmedchem.0c01567.

(65) McGuinness, D.; Malikzay, A.; Visconti, R.; Lin, K.; Bayne, M.; Monsma, F.; Lunn, C. A. Characterizing Cannabinoid CB2 Receptor Ligands Using DiscoveRx PathHunter Beta-Arrestin Assay. *J Biomol Screen* **2009**, *14* (1), 49–58. https://doi.org/10.1177/1087057108327329.

(66) Schrödinger Release 2021-2: Protein Preparation Wizard; Epik, Schrödinger, LLC, New York, NY, 2021; Impact, Schrödinger, LLC, New York, NY; Prime, Schrödinger, LLC, New York, NY, 2021.

(67) Lu, C.; Wu, C.; Ghoreishi, D.; Chen, W.; Wang, L.; Damm, W.; Ross, G. A.; Dahlgren, M. K.; Russell, E.; Von Bargen, C. D.; Abel, R.; Friesner, R. A.; Harder, E. D. OPLS4: Improving Force Field Accuracy on Challenging Regimes of Chemical Space. *J. Chem. Theory Comput.* **2021**, *17* (7), 4291–4300. https://doi.org/10.1021/acs.jctc.1c00302.

(68) Schrödinger Release 2021-2: LigPrep, Schrödinger, LLC, New York, NY, 2021.

(69) Schrödinger Release 2021-2: Glide, Schrödinger, LLC, New York, NY, 2021.

(70) Kaminski, G. A.; Friesner, R. A.; Tirado-Rives, J.; Jorgensen, W. L. Evaluation and Reparametrization of the OPLS-AA Force Field for Proteins via Comparison with Accurate Quantum Chemical Calculations on Peptides. *J. Phys. Chem. B* **2001**, *105* (28), 6474–6487. https://doi.org/10.1021/jp003919d.

(71) Genheden, S.; Ryde, U. The MM/PBSA and MM/GBSA Methods to Estimate Ligand-Binding Affinities. *Expert Opin Drug Discov* **2015**, *10* (5), 449–461. https://doi.org/10.1517/17460441.2015.1032936.

(72) Delre, P.; Caporuscio, F.; Saviano, M.; Mangiatordi, G. F. Repurposing Known Drugs as Covalent and Non-Covalent Inhibitors of the SARS-CoV-2 Papain-Like Protease. *Front Chem* **2020**, *8*, 594009. https://doi.org/10.3389/fchem.2020.594009.

Table of Content Graphic